

A parametric finite element method for a degenerate multi-phase Stefan problem with triple junctions

Tokuhiko Eto*

Harald Garcke†

Robert Nürnberg‡

Abstract

In this study, we propose a parametric finite element method for a degenerate multi-phase Stefan problem with triple junctions. This model describes the energy-driven motion of a surface cluster whose distributional solution was studied by Garcke and Sturzenhecker. We approximate the weak formulation of this sharp interface model by an unfitted finite element method that uses parametric elements for the representation of the moving interfaces. We establish existence and uniqueness of the discrete solution and prove unconditional stability of the proposed scheme. Moreover, a modification of the original scheme leads to a structure-preserving variant, in that it conserves the discrete analogue of a quantity that is preserved by the classical solution. Some numerical results demonstrate the applicability of our introduced schemes.

1 Introduction

In this study, we consider the evolution of a surface cluster $\Gamma(t)$ in \mathbb{R}^d , $d = 2, 3$, which is governed by the following system of equations for $(w(\cdot, t), \Gamma(t))$:

$$\left\{ \begin{array}{ll} \Delta w = 0 & \text{in } \Omega \setminus \Gamma(t), \quad t \in (0, T), \\ [\beta]_{b_i^-}^{b_i^+} w = -\varsigma_i \mathbf{x}_i & \text{on } \Gamma_i(t), \quad t \in (0, T), \quad i \in \mathbb{N}_{\leq I_S}, \\ [\beta]_{b_i^-}^{b_i^+} V_i = [\nabla w]_{b_i^-}^{b_i^+} \cdot \vec{\nu}_i & \text{on } \Gamma_i(t), \quad t \in (0, T), \quad i \in \mathbb{N}_{\leq I_S}, \\ \sum_{j=1}^3 \varsigma_{s_j^k} \vec{\mu}_{s_j^k} = \vec{0} & \text{on } \mathcal{T}_k(t), \quad t \in (0, T), \quad k \in \mathbb{N}_{\leq I_T}, \\ \nabla w \cdot \vec{\nu}_\Omega = 0 & \text{on } \partial\Omega, \quad t \in (0, T), \\ \Gamma(0) = \Gamma_0, & \end{array} \right. \quad (1.1)$$

where $T > 0$ is a time horizon; $\mathbb{N}_{\leq K} = \{1, \dots, K\}$ denotes the set of all natural numbers which are not larger than K for each $K \in \mathbb{N}$, and $\Omega \subset \mathbb{R}^d$ is a smooth bounded domain. The problem (1.1) represents a degenerate multi-phase Stefan problem first studied by Garcke and Sturzenhecker in [42]. In particular, the domain Ω is divided into several phases, which are separated by a surface cluster consisting of I_S surfaces that meet at I_T triple junctions.

*Université Claude Bernard Lyon 1, CNRS, Centrale Lyon, INSA Lyon, Université Jean Monnet, ICJ UMR5208, 69622 Villeurbanne, France. E-mail: eto@math.univ-lyon1.fr

†Fakultät für Mathematik, Universität Regensburg, 93040 Regensburg, Germany. E-mail: harald.garcke@ur.de

‡Dipartimento di Matematica, Università di Trento, 38123 Trento, Italy. E-mail: robert.nurnberg@unitn.it

For the representation of the evolving surface cluster $\Gamma(t)$, we adopt the notation from [40]. See Figure 1 for the sketch of an example in \mathbb{R}^2 .

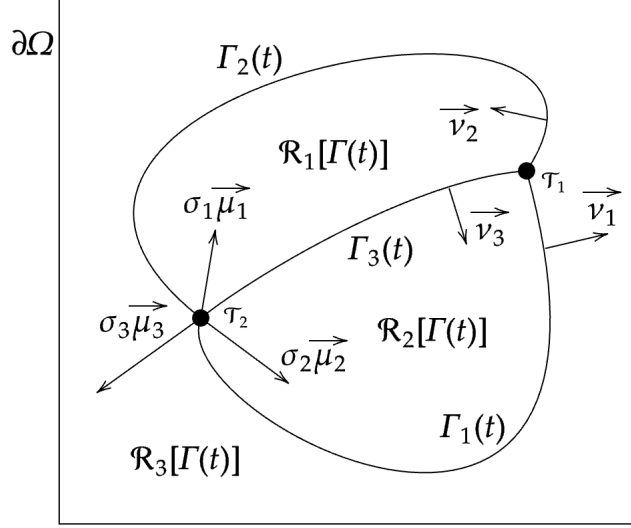


Figure 1: A surface cluster in 2d made up of three open curves and two triple junctions.

The domain Ω is split into subdomains $\mathcal{R}_\ell[\Gamma(t)]$ ($\ell \in \mathbb{N}_{\leq I_R}$) with $I_R \geq 2$ by a surface cluster $\Gamma(t) = \bigcup_{i=1}^{I_S} \Gamma_i(t)$ with $I_S \geq 1$, i.e., $\Omega = \Gamma(t) \cup \bigcup_{\ell=1}^{I_R} \mathcal{R}_\ell[\Gamma(t)]$ with $\mathcal{R}_{\ell_1}[\Gamma(t)] \cap \mathcal{R}_{\ell_2}[\Gamma(t)] = \emptyset$ if $\ell_1 \neq \ell_2$. Each $\Gamma_i(t)$ ($i \in \mathbb{N}_{\leq I_S}$) is supposed to be either a closed hypersurface without boundary or a hypersurface with boundary in Ω . $\mathcal{T}_k(t)$ ($k \in \mathbb{N}_{\leq I_T}$) denotes triple junctions at which exactly three hypersurfaces $\Gamma_{s_1^k}(t)$, $\Gamma_{s_2^k}(t)$ and $\Gamma_{s_3^k}(t)$ with $1 \leq s_1^k < s_2^k < s_3^k \leq I_S$ meet at their boundary $\bigcap_{j=1}^3 \partial \Gamma_{s_j^k}(t)$. We define a mapping $b : \mathbb{N}_{\leq I_S} \ni i \mapsto (b_i^+, b_i^-) \in (\mathbb{N}_{\leq I_R})^2$ which means that the unit normal vector field \vec{v}_i on $\Gamma_i(t)$ points from the region $\mathcal{R}_{b_i^-}[\Gamma(t)]$ into the region $\mathcal{R}_{b_i^+}[\Gamma(t)]$. We note that the regions $\mathcal{R}_\ell[\Gamma(t)]$ are not necessarily connected. To cope with this restriction, we require the mapping b to satisfy $(b_i^+, b_i^-) = (b_j^+, b_j^-)$ if $\{b_i^+, b_i^-\} = \{b_j^+, b_j^-\}$. This means that the normal direction is consistent even if two different interfaces separate the same two phases.

The parameters ς_i ($i \in \mathbb{N}_{\leq I_S}$) are positive constants which denote the surface tensions of $\Gamma_i(t)$. The parameters β_ℓ ($\ell \in \mathbb{N}_{\leq I_R}$) denote constants which, depending on the application, are related to the mass or energy contents of the phases and satisfy $\beta_{\ell_1} \neq \beta_{\ell_2}$ if $\ell_1 \neq \ell_2$. Moreover, \vec{v}_Ω denotes the outward unit normal vector field on $\partial\Omega$; \varkappa_i ($i \in \mathbb{N}_{\leq I_S}$) is the scalar mean curvature of $\Gamma_i(t)$ in the direction of \vec{v}_i , where we use the sign convention that $\varkappa_i < 0$ if $\Gamma_i(t)$ is a closed convex surface with outer normal \vec{v}_i . For a quantity q , $[q]_{b_i^-}^{b_i^+}$ denotes the jump of q across $\Gamma_i(t)$ from the b_i^- -th phase to the b_i^+ -th phase, say $[q]_{b_i^-}^{b_i^+}(x) := \lim_{\varepsilon \downarrow 0} \{q(x + \varepsilon \vec{v}_i(x)) - q(x - \varepsilon \vec{v}_i(x))\}$ for each $x \in \Gamma_i(t)$. In addition, $\vec{\mu}_i$ denotes the conormal, i.e. the intrinsic outer unit normal to $\partial\Gamma_i$, the boundary of Γ_i , that lies within the tangent plane of Γ_i , while V_i is the normal velocity of $\Gamma_i(t)$ in the direction \vec{v}_i . Finally, the cluster Γ_0 represents initial data to close the system (1.1).

The system (1.1) can be obtained as a gradient flow of the surface energy of $\Gamma(t)$ as

explained in Section 2. In the physical point of view, each interface $\Gamma_i(t)$ is a free boundary between two phases, while w is a so-called chemical potential. The fourth equation in (1.1) describes force balance conditions on the triple junction lines \mathcal{T}_k , $k \in \mathbb{N}_{\leq I_T}$. In the case of equal energy densities, they lead to the well known 120° angle conditions at triple junction lines. We observe that only differences of β_ℓ appear in the model (1.1), and so from now on we assume without loss of generality that these coefficients are normalized to satisfy $\sum_{\ell=1}^{I_R} \beta_\ell = 0$.

We note that the system (1.1) reduces to the two-phase Mullins–Sekerka model in the case $I_R = 2$. Indeed, on letting $I_R = 2$, $I_S = 1$, $I_T = 0$, $(b_1^+, b_1^-) = (1, 2)$, $\beta_1 = -0.5$ and $\beta_2 = 0.5$, we obtain that

$$\begin{cases} \Delta w = 0 & \text{in } \Omega \setminus \Gamma(t), \quad t \in (0, T), \\ [\beta]_2^1 w = -\varsigma_1 \varkappa_1 & \text{on } \Gamma_1(t), \quad t \in (0, T), \\ [\beta]_2^1 V_1 = [\nabla w]_2^1 \cdot \vec{\nu}_1 & \text{on } \Gamma_1(t), \quad t \in (0, T), \\ \nabla w \cdot \vec{\nu}_\Omega = 0 & \text{on } \partial\Omega, \quad t \in (0, T), \\ \Gamma(0) = \Gamma_0, \end{cases} \quad (1.2)$$

where $\mathcal{R}_1[\Gamma(t)]$ is the region enclosed by $\Gamma_1(t)$, and $\vec{\nu}_1$ is the inward unit normal vector field of $\Gamma_1(t)$. Meanwhile, $\mathcal{R}_2[\Gamma(t)]$ is the exterior domain, say $\mathcal{R}_2[\Gamma(t)] = \Omega \setminus \overline{\mathcal{R}_1[\Gamma(t)]}$. Since $[\beta]_2^1 = -1$, (1.2) collapses to the classical two-phase Mullins–Sekerka problem, often also called Hele–Shaw problem, [30].

The sharp interface model that we consider in this paper is a degenerate version of the multi-phase Stefan problem, and its distributional solution was first studied by Garcke and Sturzenhecker [42]. Following Luckhaus and Sturzenhecker [48], they showed existence of a distributional solution to the problem (1.1) using a minimizing movement scheme of an energy functional tailored to the multi-phase flow. The purpose of this paper is to establish a numerical scheme to compute their weak solutions.

The numerical scheme proposed in this paper is based on the parametric finite element method which is tailored to deal with the appearance of triple junctions, which is the so-called BGN method [10, 11, 12, 14]. In the latter papers, the evolution governed by the surface diffusion and the mean curvature flow with triple junction was computed. As discussed in Section 2, the multi-phase model that we consider possesses a gradient flow structure and conserves an energy-type quantity. It would be good if we could retain these structure and properties even for approximate solutions generated by a fully discrete numerical scheme. For this purpose, Bao and Zhao [6] introduced a structure-preserving parametric finite element method (SP-PFEM) for the surface diffuse flow. After that, the BGN method was combined with this structure-preserving numerical method by Bao, Garcke, Nürnberg and Zhao [3], and the surface diffuse flow with triple junctions could be handled without loss of the weighted mass conservation property. This methodology was adapted to the two-phase Mullins–Sekerka problem and the multi-phase Mullins–Sekerka problem by Nürnberg [51] and the authors [33], respectively. We note that the mathematical model that the authors [33] dealt with is different from the model (1.1) since the chemical potential of each phase is expressed as a single scalar-valued function in (1.1). For further recent works which analyzed geometric flows using the SP-PFEM, we refer the reader to [4, 5, 39, 40, 45].

Various numerical methods have been developed to address the Mullins–Sekerka problem. For the boundary integral method for the two-phase case, we refer the reader to [17, 16, 23, 49, 55]. A level-set formulation of moving boundaries together with the finite difference method was proposed in [24]. For an implementation of the method of fundamental solutions

for the two-phase Mullins–Sekerka problem in \mathbb{R}^2 , see [32]. Combination of the method of fundamental solutions and a deep-learning based approach can be found in [44], although the main focus of the paper is approximating the Dirichlet-to-Neumann map with the help of neural networks.

We also mention some numerical methods for the diffuse interface model. Numerical analysis of the scalar Cahn–Hilliard equation is dealt with in the works [7, 8, 19, 28]. Feng and Prohl [35] proposed a mixed fully discrete finite element method for the Cahn–Hilliard equation and provided error estimates between the solution of the Mullins–Sekerka problem and the approximate solution of the Cahn–Hilliard equation which are computed by their scheme. The established error bounds yielded a convergence result in [36]. Aside from the sharp interface model, the Cahn–Hilliard equation for the multi-component case has been computed in several works, see [9, 18, 34, 46, 50]. The multi-component Cahn–Hilliard equation on surfaces has recently been considered in [47]. See [20] for a study of the multi-component Cahn–Hilliard model involving concentration-dependent mobilities, and it adopted the semi-implicit scheme together with the Fourier transform to compute a discrete solution to the geometric flow.

We briefly review some analytical researches on the Mullins–Sekerka problem and its diffuse interface model. For classical solutions, Chen, Hong and Yi [25] showed the existence of a classical solution to the Mullins–Sekerka problem local-in-time in the two-dimensional case, while Escher and Simonett [31] gave a similar result in the general dimensional case. For the notion of weak solutions, Luckhaus and Sturzenhecker [48] established the existence of weak solutions to the two-phase Mullins–Sekerka problem in a distributional sense. Therein, the weak solution was obtained as a limit of a sequence of time discrete approximate solutions under the no mass loss assumption. The time implicit scheme is the basis of the approach in [21]. After that, Röger [52] removed the technical assumption of no mass loss in the case when the Dirichlet-Neumann boundary condition is imposed by using geometric measure theory. For this direction, we also find a convergence result of a minimizing movement scheme involving the Wasserstein distance of sets for the one-phase Mullins–Sekerka problem in the work by Chambolle and Laux [22]. They regarded the gradient of the chemical potential as a solenoidal vector field and constructed a sequence of approximate set-theoretic solutions. This sequence turned out to converge (up to a subsequence) to a distributional solution which was transported by the vector field.

Recently, researches which treat the boundary contact case gradually appear. For the ninety-degree contact angle case, Abels, Rauchecker and Wilke [1] showed well-posedness of the two-phase Mullins–Sekerka problem with the help of linearization approach. Meanwhile, Garcke and Rauchecker [41] carried out a stability analysis in a curved domain in \mathbb{R}^2 via a linearization approach. The ninety-degree contact angle condition was numerically computed by Eto [32] in \mathbb{R}^2 , and its outcome exhibited that the curve shortening property and the area-preserving property were satisfied even in the discrete level. Whereas, Hensel and Stinson [43] proposed a varifold solution to the two-phase Mullins–Sekerka problem with fixed contact angle condition focussing on the energy dissipation property of the model. Their definition of weak solutions was based on the maximum slope of the area functional in some topology. Fischer, Hensel, Laux and Simon [37] announced that this weak solution is unique as long as a smooth solution to the two-phase Mullins–Sekerka problem exists, although their result was restricted to the two-dimensional case, and the contact angle condition was not treated. For a gradient flow aspect of the Mullins–Sekerka flow, see e.g. [54, §3.2]. A recent study by Escher, Matioc and Matioc [29] showed well-posedness of the two-phase Mullins–Sekerka

problem in the whole domain \mathbb{R}^2 in terms of the potential method. Their result supported the mathematical model which was considered in [16, 32].

This paper is organized as follows. In Section 2, we focus on the gradient flow structure of the problem (1.1). We also confirm that a classical solution to the problem (1.1) satisfies the dissipation property of surface energy and the total energy content preserving property. In Section 3, we will construct a weak formulation of the problem (1.1). In Section 4, we will define a discrete solution to the problem (1.1) by using a parametric finite element method. We also prove existence and uniqueness of the discrete solution and unconditional stability of the proposed scheme. In Section 5, we will formulate the matrix form of the weak formulation to solve the linear system for the three-phase case. In Section 6, we will introduce a vertex normal so that the fully discrete scheme conserves the total energy content on the discrete level. In Section 7, we will carry out several numerical experiments to confirm feasibility of the proposed scheme and its accuracy. Finally, we will conclude this paper in Section 8 by summarizing the main results.

2 Gradient Flow and Energy Dissipation Properties

In a spirit of Garcke and Sturzenhecker [42], we begin by focusing on a gradient flow structure of the underlying problem (1.1). Let $E(\Gamma(t))$ be the surface energy of $\Gamma(t)$ defined by

$$E(\Gamma(t)) := \sum_{i=1}^{I_S} \int_{\Gamma_i(t)} \varsigma_i \, d\mathcal{H}^{d-1}, \quad (2.1)$$

where \mathcal{H}^{d-1} denotes the $(d-1)$ -dimensional Hausdorff measure.

Let $m \in \mathbb{R}$ be a constant which indicates the total energy content. Then, we define a function space \mathcal{M}_m and its tangential space $T_\Gamma \mathcal{M}_m$ by

$$\begin{aligned} \mathcal{M}_m &:= \left\{ (\chi_1, \dots, \chi_{I_R}) \in BV(\Omega; \{0, 1\})^{I_R} \mid \sum_{\ell=1}^{I_R} \int_{\mathcal{R}_\ell[\Gamma(t)]} \beta_\ell \chi_\ell \, d\mathcal{L}^d = m \right\}, \\ T_\Gamma \mathcal{M}_m &:= \left\{ V : \Gamma \rightarrow \mathbb{R} \mid \sum_{i=1}^{I_S} \int_{\Gamma_i} [\beta]_{b_i^-}^{b_i^+} V_i \, d\mathcal{H}^{d-1} = 0 \right\}, \end{aligned}$$

where $BV(\Omega; \{0, 1\})$ denotes the set of all functions of bounded variation on Ω taking the values in $\{0, 1\}$, and \mathcal{L}^d denotes the d -dimensional Lebesgue measure. Then, we define an inner product on $T_\Gamma \mathcal{M}_m$ by

$$\langle V_1, V_2 \rangle_{T_\Gamma \mathcal{M}_m} := \int_{\Omega} \nabla w_1 \cdot \nabla w_2 \, d\mathcal{L}^d = - \sum_{i=1}^{I_S} \int_{\Gamma_i} w_1 [\beta]_{b_i^-}^{b_i^+} V_2 \, d\mathcal{H}^{d-1},$$

where $w_k \in H^1(\Omega)$ ($k = 1, 2$) solves

$$\begin{cases} \Delta w_k = 0 & \text{in } \Omega \setminus \Gamma, \\ [\nabla w_k]_{b_i^-}^{b_i^+} \cdot \vec{\nu}_i = [\beta]_{b_i^-}^{b_i^+} V_{k,i} & \text{on } \Gamma_i, \quad \forall i \in \mathbb{N}_{\leq I_S}, \\ \nabla w_k \cdot \vec{\nu}_\Omega = 0 & \text{on } \partial\Omega. \end{cases} \quad (2.2)$$

For the definition of this inner product in the two-phase case, we refer the reader to Garcke [38]. The first variation of the energy $E(\Gamma)$ with respect to this metric on $T_\Gamma \mathcal{M}_m$ is given by

$$\nabla_{T_\Gamma \mathcal{M}_m} E(\Gamma) = -\Lambda_\Gamma^\beta \varsigma \varkappa, \quad (2.3)$$

where Λ_Γ^β denotes the Dirichlet-to-Neumann operator on Γ defined by

$$\Lambda_\Gamma^\beta f := g \quad \text{for } f \in H^{\frac{1}{2}}(\Gamma).$$

The operator $\Lambda_\Gamma^\beta f$ is defined as follows. For $f \in H^{\frac{1}{2}}(\Gamma)$, define $w \in H^1(\Omega)$ such that

$$\begin{cases} \Delta w = 0 & \text{in } \Omega \setminus \Gamma, \\ [\beta]_{b_i^-}^{b_i^+} w = f_i & \text{on } \Gamma_i, \quad \forall i \in \mathbb{N}_{\leq I_S}, \\ \nabla w \cdot \vec{\nu}_\Omega = 0 & \text{on } \partial\Omega. \end{cases} \quad (2.4)$$

Then we let $g \in H^{-\frac{1}{2}}(\Gamma)$ be such that

$$[\nabla w]_{b_i^-}^{b_i^+} \cdot \vec{\nu}_i = [\beta]_{b_i^-}^{b_i^+} g_i \quad \text{on } \Gamma_i, \quad \forall i \in \mathbb{N}_{\leq I_S}.$$

In the above, we have used the slight abuse of notation $H^{\pm\frac{1}{2}}(\Gamma) = \bigotimes_{i=1}^{I_S} H^{\pm\frac{1}{2}}(\Gamma_i)$. By the definition of Λ_Γ^β , we see that the system (1.1) can be interpreted as the geometric evolution equation:

$$V = -\Lambda_{\Gamma(t)}^\beta \varsigma \varkappa \quad \text{on } \Gamma(t), \quad t \in (0, T).$$

To observe (2.3), suppose that w solves (2.2) with this V . Assume that \tilde{w} is a solution to (2.4) with $f = -\varsigma \varkappa$, and set $g = -\Lambda_{\Gamma(t)}^\beta \varsigma \varkappa$. Then, we deduce from the transport theorem (see e.g., [2, Theorem 3.4.2]) that

$$\begin{aligned} \frac{d}{dt} E(\Gamma(t)) &= - \sum_{i=1}^{I_S} \int_{\Gamma_i(t)} \varsigma_i \varkappa_i V_i \, d\mathcal{H}^{d-1} = \sum_{i=1}^{I_S} \int_{\Gamma_i(t)} [\beta]_{b_i^-}^{b_i^+} \tilde{w} V_i \, d\mathcal{H}^{d-1} \\ &= \sum_{i=1}^{I_S} \int_{\Gamma_i(t)} \tilde{w} [\nabla w]_{b_i^-}^{b_i^+} \cdot \vec{\nu}_i \, d\mathcal{H}^{d-1} = - \int_\Omega \nabla \tilde{w} \cdot \nabla w \, d\mathcal{L}^d = \left\langle \Lambda_{\Gamma(t)}^\beta \varsigma \varkappa, V \right\rangle_{T_{\Gamma(t)} \mathcal{M}_m}. \end{aligned}$$

Therefore, we obtain the first variation (2.3). In other words, the system (1.1) also describes the gradient flow of the surface energy:

$$V = -\nabla_{T_{\Gamma(t)} \mathcal{M}_m} E(\Gamma(t)) \quad \text{on } \Gamma(t), \quad t \in (0, T). \quad (2.5)$$

We explore some properties of classical solutions of the multi-phase Stefan problem (1.1).

Proposition 2.1 (Energy dissipation). *Let $(w, \Gamma(t))$ be a classical solution of (1.1). Then, the surface energy of $\Gamma(t)$ is not increasing in time. Precisely, it holds that*

$$\frac{d}{dt} E(\Gamma(t)) = - \int_\Omega |\nabla w|^2 \, d\mathcal{L}^d.$$

Proof. We deduce from the transport theorem and the homogeneous Neumann boundary condition that

$$\begin{aligned}
\frac{d}{dt}E(\Gamma(t)) &= - \sum_{i=1}^{I_S} \int_{\Gamma_i(t)} \varsigma_i \mathcal{K}_i V_i \, d\mathcal{H}^{d-1} = \sum_{i=1}^{I_S} \int_{\Gamma_i(t)} [\beta]_{b_i^+}^{b_i^-} w V_i \, d\mathcal{H}^{d-1} \\
&= \sum_{i=1}^{I_S} \int_{\Gamma_i(t)} w [\nabla w]_{b_i^-}^{b_i^+} \cdot \vec{\nu}_i \, d\mathcal{H}^{d-1} = - \sum_{\ell=1}^{I_R} \int_{\mathcal{R}_\ell[\Gamma(t)]} |\nabla w|^2 \, d\mathcal{L}^d \\
&= - \int_{\Omega} |\nabla w|^2 \, d\mathcal{L}^d.
\end{aligned}$$

□

Proposition 2.2 (Total energy content preservation). *Let $(w, \Gamma(t))$ be a classical solution of (1.1). Then, the total energy content is preserved in time. Namely, it holds that*

$$\frac{d}{dt} \sum_{\ell=1}^{I_R} \beta_\ell \, \text{vol}(\mathcal{R}_\ell[\Gamma(t)]) = 0,$$

where $\text{vol}(\cdot) := \mathcal{L}^d(\cdot)$.

Proof. For each $\ell \in \mathbb{N}_{\leq I_R}$, let \mathcal{V}_ℓ be the normal velocity of $\partial\mathcal{R}_\ell[\Gamma(t)]$ inward to $\mathcal{R}_\ell[\Gamma(t)]$. Then, we have

$$\begin{aligned}
\frac{d}{dt} \beta_\ell \, \text{vol}(\mathcal{R}_\ell[\Gamma(t)]) &= -\beta_\ell \int_{\partial\mathcal{R}_\ell[\Gamma(t)]} \mathcal{V}_\ell \, d\mathcal{H}^{d-1} \\
&= -\beta_\ell \sum_{\substack{i \in \mathbb{N}_{\leq I_S} \\ b_i^+ = \ell}} \int_{\Gamma_i(t)} V_i \, d\mathcal{H}^{d-1} + \beta_\ell \sum_{\substack{i \in \mathbb{N}_{\leq I_S} \\ b_i^- = \ell}} \int_{\Gamma_i(t)} V_i \, d\mathcal{H}^{d-1}. \tag{2.6}
\end{aligned}$$

Summing up (2.6) over all $\ell \in \mathbb{N}_{\leq I_R}$ together with the homogeneous Neumann boundary condition, we have

$$\begin{aligned}
\frac{d}{dt} \sum_{\ell=1}^{I_R} \beta_\ell \, \text{vol}(\mathcal{R}_\ell[\Gamma(t)]) &= - \sum_{i=1}^{I_S} \int_{\Gamma_i(t)} [\beta]_{b_i^-}^{b_i^+} V_i \, d\mathcal{H}^{d-1} = - \sum_{i=1}^{I_S} \int_{\Gamma_i(t)} [\nabla w]_{b_i^-}^{b_i^+} \cdot \vec{\nu}_i \, d\mathcal{H}^{d-1} \\
&= \sum_{\ell=1}^{I_R} \int_{\mathcal{R}_\ell[\Gamma(t)]} \Delta w \, d\mathcal{L}^d = 0.
\end{aligned}$$

□

Remark 2.1. *In contrast to the multi-phase model which was dealt with in [33], we observe that the system (1.1) does not conserve the mass of each of the phases. In other words, the mathematical model (1.1) is essentially different from that in [33, Eq.(1.2)].*

3 Weak formulation

In this section, we establish a weak formulation for the degenerate multi-phase Stefan problem (1.1). We take a test function $\varphi \in H^1(\Omega)$ and multiply the first equation of (1.1) by φ . For each $\ell \in \mathbb{N}_{\leq I_R}$, we have

$$\begin{aligned} \int_{\mathcal{R}_\ell[\Gamma(t)]} \Delta w \varphi \, d\mathcal{L}^d &= \sum_{\substack{i \in \mathbb{N}_{\leq I_S} \\ b_i^+ = \ell}} \int_{\Gamma_i(t)} -(\nabla w \cdot \vec{\nu}_i) \varphi \, d\mathcal{H}^{d-1} + \sum_{\substack{i \in \mathbb{N}_{\leq I_S} \\ b_i^- = \ell}} \int_{\Gamma_i(t)} (\nabla w \cdot \vec{\nu}_i) \varphi \, d\mathcal{H}^{d-1} \\ &\quad - \int_{\mathcal{R}_\ell[\Gamma(t)]} \nabla w \cdot \nabla \varphi \, d\mathcal{L}^d. \end{aligned} \quad (3.1)$$

Summing up (3.1) over all $\ell \in \mathbb{N}_{\leq I_R}$, we have

$$\begin{aligned} 0 &= \sum_{i=1}^{I_S} \int_{\Gamma_i(t)} (-[\nabla w]_{b_i^-}^{b_i^+} \cdot \vec{\nu}_i) \varphi \, d\mathcal{H}^{d-1} - \int_{\Omega} \nabla w \cdot \nabla \varphi \, d\mathcal{L}^d \\ &= \sum_{i=1}^{I_S} \int_{\Gamma_i(t)} -[\beta]_{b_i^-}^{b_i^+} V_i \varphi \, d\mathcal{H}^{d-1} - \int_{\Omega} \nabla w \cdot \nabla \varphi \, d\mathcal{L}^d, \end{aligned}$$

where we have used the third equation of the system (1.1) to transform $[\nabla w]_{b_i^-}^{b_i^+} \cdot \vec{\nu}_i$ to $[\beta]_{b_i^-}^{b_i^+} V_i$. Meanwhile, a weak formulation for the Gibbs–Thomson law of the system (1.1) is straightforward:

$$\sum_{i=1}^{I_S} \int_{\Gamma_i(t)} ([\beta]_{b_i^-}^{b_i^+} w + \varsigma_i \varkappa_i) \xi \, d\mathcal{H}^{d-1} = 0 \quad \forall \xi \in L^2(\Gamma(t)).$$

Finally, let us obtain a weak formulation for the curvature vector. Let $\text{id} : \mathbb{R}^d \rightarrow \mathbb{R}^d$ be the identity function. Then, we know the following formula for the curvature vector:

$$\Delta_\Gamma \vec{\text{id}} = \varkappa_i \vec{\nu}_i \quad \text{on } \Gamma_i(t), \quad (3.2)$$

where Δ_Γ denotes the Laplace–Beltrami operator defined by $\nabla_\Gamma \cdot \nabla_\Gamma$ by using the surface gradient ∇_Γ . We now introduce a test function space for (3.2) by

$$\underline{V}(\Gamma(t)) := \left\{ (\vec{\eta}_1, \dots, \vec{\eta}_{I_S}) \in \bigotimes_{i=1}^{I_S} H^1(\Gamma_i(t); \mathbb{R}^d) \mid \vec{\eta}_{s_1^k} = \vec{\eta}_{s_2^k} = \vec{\eta}_{s_3^k} \quad \text{on } \mathcal{T}_k(t), \quad \forall k \in \mathbb{N}_{\leq I_T} \right\}.$$

Multiplying (3.2) with $\varsigma_i \vec{\eta}_i$, for an arbitrary $\vec{\eta} \in \underline{V}(\Gamma(t))$, integrating over $\Gamma_i(t)$, summing and performing integration by parts yields

$$\begin{aligned}
& \sum_{i=1}^{I_S} \int_{\Gamma_i(t)} \varsigma_i \kappa_i \vec{\nu}_i \cdot \vec{\eta}_i \, d\mathcal{H}^{d-1} = \sum_{i=1}^{I_S} \int_{\Gamma_i(t)} \varsigma_i \Delta_{\Gamma} \vec{\text{id}} \cdot \vec{\eta}_i \, d\mathcal{H}^{d-1} \\
& = \sum_{i=1}^{I_S} \left(\int_{\partial \Gamma_i(t)} \varsigma_i (\nabla_{\Gamma} \vec{\text{id}} \vec{\eta}_i) \cdot \vec{\mu}_i \, d\mathcal{H}^{d-2} - \int_{\Gamma_i(t)} \varsigma_i \nabla_{\Gamma} \vec{\text{id}} \cdot \nabla_{\Gamma} \vec{\eta}_i \, d\mathcal{H}^{d-1} \right) \\
& = \sum_{k=1}^{I_T} \int_{\mathcal{T}_k(t)} \sum_{j=1}^3 \varsigma_{s_j^k} (\nabla_{\Gamma} \vec{\text{id}} \vec{\eta}_{s_j^k}) \cdot \vec{\mu}_{s_j^k} \, d\mathcal{H}^{d-2} - \sum_{i=1}^{I_S} \int_{\Gamma_i(t)} \varsigma_i \nabla_{\Gamma} \vec{\text{id}} \cdot \nabla_{\Gamma} \vec{\eta}_i \, d\mathcal{H}^{d-1} \\
& = \sum_{k=1}^{I_T} \int_{\mathcal{T}_k(t)} (\nabla_{\Gamma} \vec{\text{id}} \vec{\eta}_{s_1^k}) \sum_{j=1}^3 \varsigma_{s_j^k} \vec{\mu}_{s_j^k} \, d\mathcal{H}^{d-2} - \sum_{i=1}^{I_S} \int_{\Gamma_i(t)} \varsigma_i \nabla_{\Gamma} \vec{\text{id}} \cdot \nabla_{\Gamma} \vec{\eta}_i \, d\mathcal{H}^{d-1} \\
& = - \sum_{i=1}^{I_S} \int_{\Gamma_i(t)} \varsigma_i \nabla_{\Gamma} \vec{\text{id}} \cdot \nabla_{\Gamma} \vec{\eta}_i \, d\mathcal{H}^{d-1}.
\end{aligned}$$

For the integrals on the triple junctions $\mathcal{T}_k(t)$ we have first used that $\vec{\eta} \in \underline{V}(\Gamma(t))$, and then noticed that they vanish due to Young's law, which is the fourth condition of the system (1.1). For later use, we define the inner products in Ω and on $\Gamma(t)$ by

$$\langle u, v \rangle_{\Omega} := \int_{\Omega} u v \, d\mathcal{L}^d \quad \text{and} \quad \langle u, v \rangle_{\Gamma(t)} := \sum_{i=1}^{I_S} \int_{\Gamma_i(t)} u_i v_i \, d\mathcal{H}^{d-1}.$$

We conclude this section by summarizing the weak formulation of the system, where from now on we use the short-hand notation κ_{ς} defined by $\kappa_{\varsigma}|_{\Gamma_i(t)} = \varsigma_i \kappa_i$ for $i \in \mathbb{N}_{\leq I_S}$. The weak formulation of problem (1.1) amounts to finding a time-dependent pair $(w, \Gamma(t))$ of a diffuse function w and a surface cluster $\Gamma(t)$ such that for each $t \in (0, T)$:

Motion law: For all $\varphi \in H^1(\Omega)$, it holds that

$$\langle \nabla w, \nabla \varphi \rangle_{\Omega} + \sum_{i=1}^{I_S} [\beta]_{b_i^-}^{b_i^+} \langle V_i, \varphi \rangle_{\Gamma_i(t)} = 0. \tag{3.3a}$$

Gibbs–Thomson law: For all $\xi \in L^2(\Gamma(t))$, it holds that

$$\sum_{i=1}^{I_S} \left\langle [\beta]_{b_i^-}^{b_i^+} w + \kappa_{\varsigma}, \xi \right\rangle_{\Gamma_i(t)} = 0. \tag{3.3b}$$

Curvature vector: For all $\vec{\eta} \in \underline{V}(\Gamma(t))$, it holds that

$$\langle \kappa_{\varsigma} \vec{\nu}, \vec{\eta} \rangle_{\Gamma(t)} + \langle \varsigma \nabla_{\Gamma} \vec{\text{id}}, \nabla_{\Gamma} \vec{\eta} \rangle_{\Gamma(t)} = 0. \tag{3.3c}$$

4 Parametric finite element method

In this section, we propose a parametric finite element method for the degenerate multi-phase Stefan problem (1.1) based on the weak formulation (3.3). For the presentation of the necessary finite element spaces we closely follow the notation from [3], see also [14].

We split the interval $[0, T]$ into M sub-intervals $[t_{m-1}, t_m]$ with $1 \leq m \leq M$ whose lengths are equal to τ_m . Then, we construct a fully discrete scheme which yields an approximate solution $(W^{m+1}, \vec{X}^{m+1}, \kappa_\zeta^{m+1})$, provided that the previous discrete cluster Γ^m is given, with $\Gamma^{m+1} = \vec{X}^{m+1}(\Gamma^m)$. In order to describe Γ^m , and the discrete matching conditions that have to hold on the triple junction, we let Υ_i^h ($i \in \mathbb{N}_{\leq I_S}$) be polyhedral reference surfaces with $\overline{\Upsilon_i^h} = \bigcup_{j=1}^{J_i} \overline{\sigma_{i,j}}$, where $\{\sigma_{i,j}\}_{j=1}^{J_i}$ is a family of mutually disjoint open $(d-1)$ -simplices with vertices $\{\vec{q}_{i,k}\}_{k=1}^{K_i}$ vertices.

Moreover, we assume that each boundary $\partial \Upsilon_i^h$ is split into I_P^i sub-boundaries $\partial_p \Upsilon_i^h$ ($p \in \mathbb{N}_{\leq I_P^i}$), and each sub-boundary $\partial_p \Upsilon_i^h$ corresponds to the parameterization of a triple junction. In particular, we will let $\Gamma_i^m = \vec{\mathfrak{X}}_i^m(\Upsilon_i^h)$, so that the triple junction \mathcal{T}_k , where the surfaces $\Gamma_{s_1^k}(t)$, $\Gamma_{s_2^k}(t)$, $\Gamma_{s_3^k}(t)$ meet, is approximated by the images of $\vec{\mathfrak{X}}^m$ on $\partial_{p_1^k} \Upsilon_{s_1^k}^h$, $\partial_{p_2^k} \Upsilon_{s_2^k}^h$, $\partial_{p_3^k} \Upsilon_{s_3^k}^h$. To this end, we have to ensure that these sub-boundaries perfectly match up on the triple junctions, and in particular contain the same number of vertices. Hence, we assume that for every $k \in \mathbb{N}_{\leq I_T}$, it holds that

$$Z_k := \#Q_{s_1^k, p_1^k} = \#Q_{s_2^k, p_2^k} = \#Q_{s_3^k, p_3^k}, \quad (4.1)$$

where $Q_{s,p} := \left\{ \vec{q}_{s,\ell} \right\}_{\ell=1}^{K_s} \cap \partial_p \Upsilon_s^h$ denotes the set of vertices belonging to the boundary patch $\partial_p \Upsilon_s^h$. Then we assume in addition that there exist bijections $\varrho_r^k : \mathbb{N}_{\leq Z_k} \rightarrow Q_{s_r^k, p_r^k}$ ($r = 1, 2, 3$) such that $(\varrho_r^k(1), \dots, \varrho_r^k(Z_k))$ ($r = 1, 2, 3$) are ordered sequences of the vertices.

Let

$$\begin{aligned} \underline{V}^h(\Upsilon^h) &:= \left\{ (\vec{\mathfrak{X}}_1, \dots, \vec{\mathfrak{X}}_{I_S}) \in \bigotimes_{i=1}^{I_S} C(\overline{\Upsilon_i^h}; \mathbb{R}^d) \mid \vec{\mathfrak{X}}_i|_{\sigma_{i,j}} \text{ is affine } \forall j \in \mathbb{N}_{\leq J_i}, \forall i \in \mathbb{N}_{\leq I_S}, \right. \\ &\quad \left. \text{and } \vec{\mathfrak{X}}_{s_1^k}(\varrho_1^k(z)) = \vec{\mathfrak{X}}_{s_2^k}(\varrho_2^k(z)) = \vec{\mathfrak{X}}_{s_3^k}(\varrho_3^k(z)) \quad \forall z \in \mathbb{N}_{\leq Z_k}, \forall k \in \mathbb{N}_{\leq I_T} \right\}. \end{aligned}$$

Then, for each $m \geq 0$ and $\vec{\mathfrak{X}}^m \in V^h(\Upsilon^h)$, we define $\Gamma^m := \vec{\mathfrak{X}}^m(\Upsilon^h)$ with $\Gamma_i^m = \vec{\mathfrak{X}}_i^m(\Upsilon_i^h)$, $\sigma_{i,j}^m := \vec{\mathfrak{X}}_i^m(\sigma_{i,j})$ and $\vec{q}_{i,k}^m := \vec{\mathfrak{X}}_i^m(\vec{q}_{i,k})$. The discrete triple junctions \mathcal{T}_k^m ($k \in \mathbb{N}_{\leq I_T}$) are defined by $\mathcal{T}_k^m := \left\{ \vec{\mathfrak{X}}_{s_1^k}^m(\varrho_1^k(z)) \mid z \in \mathbb{N}_{\leq Z_k} \right\}$. We visualize an example discrete surface cluster in Figure 2.

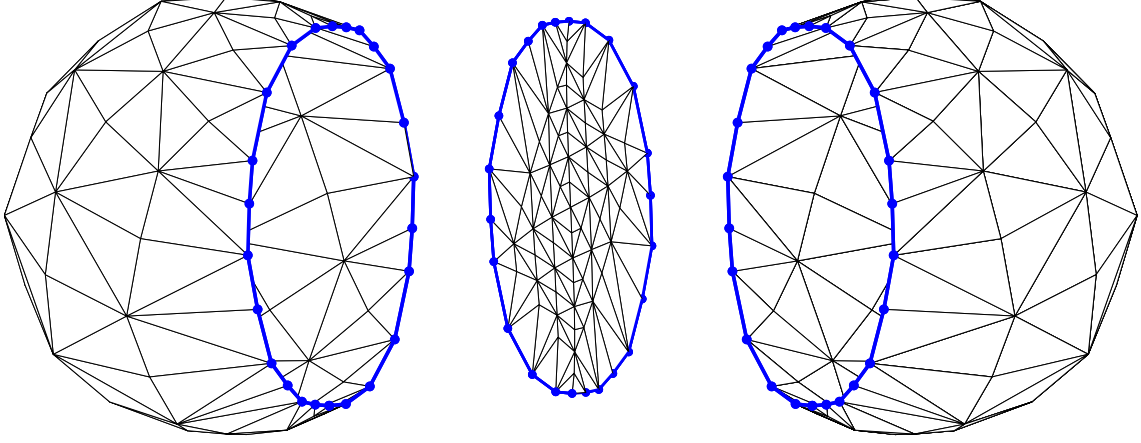


Figure 2: Example triangulation Γ^m of a triple bubble with polygonal triple junction line \mathcal{T}_1^m , where here $Z_1 = 24$.

Let us define finite element spaces from where we will seek approximate solutions. Let \mathcal{T}^m be a triangulation of $\bar{\Omega}$. Then, an approximation solution W^{m+1} is sought in the finite element space defined by

$$S^m := \left\{ v \in C(\bar{\Omega}) \mid v|_o \text{ is affine } \forall o \in \mathcal{T}^m \right\}.$$

On the polyhedral surface Γ^m we introduce finite element spaces defined by

$$\begin{aligned} V^h(\Gamma_i^m) &:= \left\{ v \in C(\Gamma_i^m) \mid v|_{\sigma_{i,j}^m} \text{ is affine } \forall j \in \mathbb{N}_{\leq J_i} \right\}, \quad i \in \mathbb{N}_{\leq I_S}, \\ \underline{V}^h(\Gamma_i^m) &:= \left\{ \mathbf{v} = (v_1, \dots, v_d) \in C(\Gamma_i^m; \mathbb{R}^d) \mid v_k \in V^h(\Gamma_i^m) \quad \forall k \in \mathbb{N}_{\leq d} \right\}, \quad i \in \mathbb{N}_{\leq I_S}. \end{aligned}$$

For later use, we also define

$$V_0^h(\Gamma_i^m) := \left\{ v \in V^h(\Gamma_i^m) \mid v = 0 \quad \text{on} \quad \partial\Gamma_i^m \right\}, \quad (4.2)$$

and let $\{\Phi_{i,k}^{m,0}\}_{k=1}^{K_i^0}$ be the standard basis of $V_0^h(\Gamma_i^m)$, so that $\Phi_{i,k}^{m,0}(\bar{q}_{i,\ell}^m) = \delta_{k\ell}$, $k, \ell \in \mathbb{N}_{\leq K_i^0}$.

Then, the approximate solutions \vec{X}^{m+1} and κ_ζ^{m+1} are respectively sought in the finite element spaces defined by

$$\begin{aligned} \underline{V}^h(\Gamma^m) &:= \left\{ (\vec{X}_1, \dots, \vec{X}_{I_S}) \in \bigotimes_{i=1}^{I_S} \underline{V}^h(\Gamma_i^m) \mid \vec{X}_{s_1^k} = \vec{X}_{s_2^k} = \vec{X}_{s_3^k} \quad \text{on} \quad \mathcal{T}_k^m, \forall k \in \mathbb{N}_{\leq I_T} \right\}, \\ V^h(\Gamma^m) &:= \bigotimes_{i=1}^{I_S} V^h(\Gamma_i^m). \end{aligned}$$

We now define the normal vector of each simplex $\sigma_{i,j}^m$. To this end, let $\{\bar{q}_{i,j,\ell}^m\}_{\ell=1}^d$ be the vertices of $\sigma_{i,j}^m$, and ordered with the same orientation for all $\sigma_{i,j}^m$, $j \in \mathbb{N}_{\leq J_i}$. Then we define

$$\vec{\nu}_{i,j}^m := \frac{\vec{A}\{\sigma_{i,j}^m\}}{|\vec{A}\{\sigma_{i,j}^m\}|} \quad \text{with} \quad \vec{A}\{\sigma_{i,j}^m\} := \begin{cases} (\bar{q}_{i,j,2}^m - \bar{q}_{i,j,1}^m)^\perp & \text{if } d = 2, \\ (\bar{q}_{i,j,2}^m - \bar{q}_{i,j,1}^m) \wedge (\bar{q}_{i,j,3}^m - \bar{q}_{i,j,1}^m) & \text{if } d = 3, \end{cases}$$

where $|\cdot| = \mathcal{H}^{d-1}(\cdot)$; the symbol \wedge denotes the wedge product, and $v^\perp := (-v_2, v_1)^T$ for $v = (v_1, v_2)^T \in \mathbb{R}^2$. Let $\vec{\nu}_i^m$ be the normal vector on Γ_i^m which equals $\vec{\nu}_{i,j}^m$ on $\sigma_{i,j}^m$.

Let us define the mass lumped inner product of two piecewise continuous functions u and v on Γ_i^m by

$$\langle u, v \rangle_{\Gamma_i^m}^h := \frac{1}{d} \sum_{j=1}^{J_i} |\sigma_{i,j}^m| \sum_{k=1}^d \lim_{\sigma_{i,j}^m \ni \vec{q} \rightarrow \vec{q}_{i,j,k}^m} (uv)(\vec{q}) \quad i \in \mathbb{N}_{\leq I_S}.$$

Using this, we define the mass lumped inner product on Γ^m by

$$\langle u, v \rangle_{\Gamma^m}^h := \sum_{i=1}^{I_S} \langle u_i, v_i \rangle_{\Gamma_i^m}^h. \quad (4.3)$$

Meanwhile, we will write the natural L^2 -inner product as follows:

$$\langle u, v \rangle_{\Gamma^m} = \sum_{i=1}^{I_S} \langle u_i, v_i \rangle_{\Gamma_i^m} = \sum_{i=1}^{I_S} \int_{\Gamma_i^m} u_i v_i d\mathcal{H}^{d-1}.$$

The notion of these inner products can be extended for two vector- and tensor-valued functions. The vertex normal $\vec{\omega}_i^m \in \underline{V}^h(\Gamma_i^m)$ on Γ_i^m is defined in terms of the L^2 projection as follows:

$$\langle \vec{\omega}_i^m, \vec{\xi} \rangle_{\Gamma_i^m}^h = \langle \vec{\nu}_i^m, \vec{\xi} \rangle_{\Gamma_i^m}^h, \quad \forall \vec{\xi} \in \underline{V}^h(\Gamma_i^m) \quad i \in \mathbb{N}_{\leq I_S}.$$

We are now in the position to introduce our finite element approximation for the weak formulation (3.3).

For $m \geq 0$, given Γ^m , find $(W^{m+1}, \vec{X}^{m+1}, \kappa_\zeta^{m+1}) \in S^m \times \underline{V}^h(\Gamma^m) \times V^h(\Gamma^m)$ such that the following three conditions hold:

Motion law: For all $\varphi \in S^m$, it holds that

$$\langle \nabla W^{m+1}, \nabla \varphi \rangle_\Omega + \sum_{i=1}^{I_S} [\beta]_{b_i^-}^{b_i^+} \left\langle \pi_i^h \left[\frac{\vec{X}_i^{m+1} - \text{id}}{\tau_m} \cdot \vec{\omega}_i^m \right], \varphi \right\rangle_{\Gamma_i^m}^{(h)} = 0. \quad (4.4a)$$

Gibbs–Thomson law: For all $\xi \in V^h(\Gamma^m)$, it holds that

$$\langle \kappa_\zeta^{m+1}, \xi \rangle_{\Gamma^m}^h + \sum_{i=1}^{I_S} [\beta]_{b_i^-}^{b_i^+} \langle W^{m+1}, \xi \rangle_{\Gamma_i^m}^{(h)} = 0. \quad (4.4b)$$

Curvature vector: For all $\vec{\eta} \in \underline{V}^h(\Gamma^m)$, it holds that

$$\langle \kappa_\zeta^{m+1} \vec{\omega}^m, \vec{\eta} \rangle_{\Gamma^m}^h + \left\langle \varsigma \nabla_\Gamma \vec{X}^{m+1}, \nabla_\Gamma \vec{\eta} \right\rangle_{\Gamma^m} = 0, \quad (4.4c)$$

where $\pi_i^h : C(\Gamma_i^m) \rightarrow V^h(\Gamma_i^m)$ denotes the standard interpolation operator, and set $\Gamma^{m+1} = \vec{X}^{m+1}(\Gamma^m)$. Above, and in what follows, the notation $\cdot^{(h)}$ means an expression with or without the superscript h . That is, (4.4) represents two different schemes. When the superscript h appears, we use the mass lumped inner product introduced in (4.3), while the inner products without the superscript h are computed by true integration.

Before proving existence and uniqueness of (4.4), we impose a technical assumption on the surface cluster. This assumption is analogous to that in [33, Assumption 1].

Assumption 4.1. For every $i \in \mathbb{N}_{\leq I_S}$, it holds that

$$\text{span} \left\{ \vec{\omega}_i^m(\vec{q}_{i,k}^m) \mid j \in \mathbb{N}_{\leq K_i^0} \right\} \neq \{\vec{0}\}.$$

Moreover, we assume that

$$\text{span} \left\{ \sum_{i=1}^{I_S} [\beta]_{b_i^-}^{b_i^+} \langle \vec{\omega}_i^m, \varphi \rangle_{\Gamma_i^m}^{(h)} \mid \varphi \in S^m \right\} = \mathbb{R}^d.$$

The first assumption says that, for each $i \in \mathbb{N}_{\leq I_S}$, amongst all the non-boundary vertex normals on Γ_i^m , there should be at least one nonzero vector. The second condition in Assumption 4.1, on the other hand, is a very mild constraint on the interaction between bulk and interface meshes. See [33, Ass. 1] and [15, Ass. 108] for very similar assumptions.

Theorem 4.1 (Existence and uniqueness). *Let $\vec{X}^m \in \underline{V}^h(\Gamma^m)$ and S^m be such that Assumption 4.1 holds. Then, there exists a unique solution $(W^{m+1}, \vec{X}^{m+1}, \kappa_\zeta^{m+1}) \in S^m \times \underline{V}^h(\Gamma^m) \times V^h(\Gamma^m)$ to (4.4).*

Proof. Since the system (4.4) is linear and finite dimensional, with as many unknowns as equations, the existence of a solution is directly deduced from the uniqueness of the solution. To show the uniqueness, we need to prove that only the trivial solution satisfies the homogeneous system.

Suppose that $(W, \vec{X}, \kappa_\zeta) \in S^m \times \underline{V}^h(\Gamma^m) \times V^h(\Gamma^m)$ satisfies

$$\tau_m \langle \nabla W, \nabla \varphi \rangle_\Omega + \sum_{i=1}^{I_S} [\beta]_{b_i^-}^{b_i^+} \left\langle \pi_i^h [\vec{X} \cdot \vec{\omega}_i^m], \varphi \right\rangle_{\Gamma_i^m}^{(h)} = 0 \quad \forall \varphi \in S^m, \quad (4.5a)$$

$$\langle \kappa_\zeta, \xi \rangle_{\Gamma^m}^h + \sum_{i=1}^{I_S} [\beta]_{b_i^-}^{b_i^+} \langle W, \xi \rangle_{\Gamma_i^m}^{(h)} = 0 \quad \forall \xi \in V^h(\Gamma^m), \quad (4.5b)$$

$$\langle \kappa_\zeta \vec{\omega}^m, \vec{\eta} \rangle_{\Gamma^m}^h + \left\langle \varsigma \nabla_\Gamma \vec{X}, \nabla_\Gamma \vec{\eta} \right\rangle_{\Gamma^m} = 0 \quad \forall \vec{\eta} \in \underline{V}^h(\Gamma^m). \quad (4.5c)$$

We choose $\varphi = W$ in (4.5a), $\xi = \pi^h [\vec{X} \cdot \vec{\omega}^m]$ in (4.5b) and $\vec{\eta} = \vec{X}$ in (4.5c) to obtain

$$\tau_m \|\nabla W\|_2^2 + \sum_{i=1}^{I_S} [\beta]_{b_i^-}^{b_i^+} \left\langle \pi_i^h [\vec{X} \cdot \vec{\omega}_i^m], W \right\rangle_{\Gamma_i^m}^{(h)} = 0, \quad (4.6)$$

$$\left\langle \kappa_\zeta, \pi^h [\vec{X} \cdot \vec{\omega}^m] \right\rangle_{\Gamma^m}^h + \sum_{i=1}^{I_S} [\beta]_{b_i^-}^{b_i^+} \left\langle W, \pi_i^h [\vec{X} \cdot \vec{\omega}_i^m] \right\rangle_{\Gamma_i^m}^{(h)} = 0, \quad (4.7)$$

$$\left\langle \kappa_\zeta \vec{\omega}^m, \vec{X} \right\rangle_{\Gamma^m}^h + \left\langle \varsigma \nabla_\Gamma \vec{X}, \nabla_\Gamma \vec{X} \right\rangle_{\Gamma^m} = 0. \quad (4.8)$$

Combining (4.6), (4.7) and (4.8), we have

$$\tau_m \|\nabla W\|_2^2 + \left\langle \varsigma \nabla_\Gamma \vec{X}, \nabla_\Gamma \vec{X} \right\rangle_{\Gamma^m} = 0.$$

The left-hand side of the above equation is non-negative, and hence we deduce that W and \vec{X} are constant, say $W \equiv W_c$ and $\vec{X} \equiv \vec{X}_c$. We deduce from (4.5a) that

$$\vec{X}_c \cdot \sum_{i=1}^{I_S} [\beta]_{b_i^-}^{b_i^+} \langle \vec{\omega}_i^m, \varphi \rangle_{\Gamma_i^m}^{(h)} = 0 \quad \forall \varphi \in S^m.$$

By the second hypothesis of Assumption 4.1, we have $\vec{X} \equiv \vec{X}_c = \vec{0}$. Meanwhile, we deduce from (4.5b) that

$$\kappa_{\varsigma,i} \equiv W_c [\beta]_{b_i^-}^{b_i^+} \quad \forall i \in \mathbb{N}_{\leq I_S}, \quad (4.9)$$

and hence κ_{ς} is constant on each surface Γ_i^m . On recalling (4.2), we now choose in (4.5c) the test function $\vec{\eta} \in \underline{V}^h(\Gamma^m)$ defined by $\vec{\eta}_i = \kappa_{\varsigma,i} \vec{z}_i^m$, where $\vec{z}_i^m := \sum_{k=1}^{K_i^0} \Phi_{i,k}^{m,0} \vec{\omega}_i^m(\vec{q}_{i,k}^m)$ for $i \in \mathbb{N}_{\leq I_S}$. On recalling that $\vec{X} = \vec{0}$, we hence obtain

$$0 = \sum_{i=1}^{I_S} (\kappa_{\varsigma,i})^2 \langle \vec{\omega}_i^m, \vec{z}_i^m \rangle_{\Gamma_i^m}^h = \sum_{i=1}^{I_S} (\kappa_{\varsigma,i})^2 \langle \vec{z}_i^m, \vec{z}_i^m \rangle_{\Gamma_i^m}^h.$$

Therefore, the first condition in Assumption 4.1 yields that $\kappa_{\varsigma,i} = 0$ for every $i \in \mathbb{N}_{\leq I_S}$, and hence $\kappa_{\varsigma} \equiv 0$. In addition, (4.9) implies that $W \equiv W_c = 0$ since $[\beta]_{b_i^-}^{b_i^+} \neq 0$ for all $i \in \mathbb{N}_{\leq I_S}$. This completes the proof. \square

Theorem 4.2 (Unconditional stability). *Let $(W^{m+1}, \vec{X}^{m+1}, \kappa_{\varsigma}^{m+1}) \in S^m \times \underline{V}^h(\Gamma^m) \times V^h(\Gamma^m)$ be a solution to (4.4). Then*

$$E(\Gamma^{m+1}) + \tau_m \|\nabla W^{m+1}\|_2^2 \leq E(\Gamma^m),$$

where we recall from (2.1) that $E(\Gamma^m) = \sum_{i=1}^{I_S} \varsigma_i |\Gamma_i^m|$.

Proof. Substituting $\varphi = W^{m+1}$ in (4.4a) and $\xi := \pi^h \left[\frac{\vec{X}^{m+1} - \text{id}}{\tau_m} \cdot \vec{\omega}^m \right]$ in (4.4b), we have

$$\begin{aligned} \|\nabla W^{m+1}\|_2^2 &= \frac{1}{\tau_m} \left\langle \kappa_{\varsigma}^{m+1}, \pi^h \left[\left(\vec{X}^{m+1} - \text{id} \right) \cdot \vec{\omega}^m \right] \right\rangle_{\Gamma^m}^h \\ &= \frac{1}{\tau_m} \left\langle \kappa_{\varsigma}^{m+1} \vec{\omega}^m, \vec{X}^{m+1} - \text{id} \right\rangle_{\Gamma^m}^h. \end{aligned} \quad (4.10)$$

Meanwhile, we choose $\vec{\eta} = \vec{X}^{m+1} - \text{id} \in \underline{V}^h(\Gamma^m)$ in (4.4c) to obtain

$$\left\langle \kappa_{\varsigma}^{m+1} \vec{\omega}^m, \vec{X}^{m+1} - \text{id} \right\rangle_{\Gamma^m}^h = - \left\langle \varsigma \nabla_{\Gamma} \vec{X}^{m+1}, \nabla_{\Gamma} (\vec{X}^{m+1} - \text{id}) \right\rangle_{\Gamma^m}. \quad (4.11)$$

We now recall [15, Lemma 57], which states that

$$\left\langle \nabla_{\Gamma} \vec{X}_i^{m+1}, \nabla_{\Gamma} (\vec{X}_i^{m+1} - \text{id}) \right\rangle_{\Gamma_i^m} \geq |\Gamma_i^{m+1}| - |\Gamma_i^m|, \quad (4.12)$$

for $i \in \mathbb{N}_{\leq I_S}$. Multiplying (4.12) with ς_i , summing and combining with (4.10) and (4.11) yields

$$\tau_m \|\nabla W^{m+1}\|_2^2 = - \left\langle \varsigma \nabla_{\Gamma} \vec{X}^{m+1}, \nabla_{\Gamma} (\vec{X}^{m+1} - \text{id}) \right\rangle_{\Gamma^m} \leq -E(\Gamma^{m+1}) + E(\Gamma^m).$$

\square

5 Matrix form of the linear system

In this section, we derive a matrix form of the linear system induced by the finite element approximation (4.4) at each time step. To facilitate understanding, we first concentrate on the two-dimensional three-phase example shown in Figure 1. Namely, we consider a curve network with $I_R = 3$, $I_S = 3$, $I_T = 2$, $(b_1^+, b_1^-) = (3, 2)$, $(b_2^+, b_2^-) = (1, 3)$ and $(b_3^+, b_3^-) = (2, 1)$.

Given Γ^m , let $(W^{m+1}, \kappa_\zeta^{m+1}, \vec{X}^m + \delta \vec{X}^{m+1}) \in S^m \times V^h(\Gamma^m) \times \underline{V}^h(\Gamma^m)$ be the unique solution of (4.4). Let K_Ω^m and K_c^m ($c \in \mathbb{N}_{\leq I_S}$) be the number of all vertices on \mathcal{T}^m and Γ_c^m , respectively. We let $K_\Gamma^m := \sum_{c=1}^{I_S} K_c^m$. In the sequel, we will regard $(W^{m+1}, \kappa_\zeta^{m+1}, \delta \vec{X}^{m+1})$ as their coefficients with respect to the basis functions $\{\Psi_i^m\}_{1 \leq i \leq K_\Omega^m}$ and $\{\{\Phi_{c,\ell}^m\}_{1 \leq \ell \leq K_c^m}\}_{c=1}^{I_S}$ of S^m and $V^h(\Gamma^m)$, respectively. We also define the orthogonal projection $\underline{P} : (\mathbb{R}^d)^K \rightarrow \underline{\mathbb{X}}$ onto the Euclidean space associated with $\underline{V}^h(\Gamma^m)$, see [14, p. 211]. Then, the solution of (4.4) can be written as $(W^{m+1}, \kappa_\zeta^{m+1}, \vec{X}^m + \underline{P} \delta \vec{X}^{m+1})$, where $(W^{m+1}, \kappa_\zeta^{m+1}, \delta \vec{X}^{m+1})$ solves the following linear system:

$$\begin{pmatrix} \tau_m A_\Omega & O & \vec{N}_{\Omega,\Gamma}^T \underline{P} \\ B_{\Omega,\Gamma} & C_\Gamma & O \\ O & \underline{P} \vec{D}_\Gamma & \underline{P} \underline{E}_\Gamma \underline{P} \end{pmatrix} \begin{pmatrix} W^{m+1} \\ \kappa_\zeta^{m+1} \\ \delta \vec{X}^{m+1} \end{pmatrix} = \begin{pmatrix} O \\ O \\ -\underline{P} \underline{E}_\Gamma \underline{P} \vec{X}^m \end{pmatrix}, \quad (5.1)$$

where $A_\Omega \in \mathbb{R}^{K_\Omega^m \times K_\Omega^m}$, $\vec{N}_{\Omega,\Gamma} \in (\mathbb{R}^d)^{K_\Gamma^m \times K_\Omega^m}$, $B_{\Omega,\Gamma} \in \mathbb{R}^{K_\Gamma^m \times K_\Omega^m}$, $C_\Gamma \in \mathbb{R}^{K_\Gamma^m \times K_\Gamma^m}$, $\vec{D}_\Gamma \in (\mathbb{R}^d)^{K_\Gamma^m \times K_\Gamma^m}$ and $\underline{E}_\Gamma \in (\mathbb{R}^{d \times d})^{K_\Gamma^m \times K_\Gamma^m}$ are defined by

$$\vec{N}_{\Omega,\Gamma} := \begin{pmatrix} [\beta]_{b_1^-}^{b_1^+} \vec{N}_1 \\ [\beta]_{b_2^-}^{b_2^+} \vec{N}_2 \\ [\beta]_{b_3^-}^{b_3^+} \vec{N}_3 \end{pmatrix}, \quad B_{\Omega,\Gamma} := \begin{pmatrix} [\beta]_{b_1^-}^{b_1^+} B_1 \\ [\beta]_{b_2^-}^{b_2^+} B_2 \\ [\beta]_{b_3^-}^{b_3^+} B_3 \end{pmatrix}, \quad C_\Gamma := \begin{pmatrix} C_1 & O & O \\ O & C_2 & O \\ O & O & C_3 \end{pmatrix},$$

$$\vec{D}_\Gamma := \begin{pmatrix} \vec{D}_1 & O & O \\ O & \vec{D}_2 & O \\ O & O & \vec{D}_3 \end{pmatrix}, \quad \underline{E}_\Gamma := \begin{pmatrix} \varsigma_1 \underline{E}_1 & O & O \\ O & \varsigma_2 \underline{E}_2 & O \\ O & O & \varsigma_3 \underline{E}_3 \end{pmatrix}$$

with

$$\begin{aligned} [A_\Omega]_{i,j} &:= \langle \nabla \Psi_j^m, \nabla \Psi_i^m \rangle_\Omega, & [\vec{N}_c]_{\ell,i} &:= \langle \Phi_{c,\ell}^m, \Psi_i^m \rangle_{\Gamma_c^m}^{(h)} \vec{\omega}_{c,\ell}^m, \\ [B_c]_{k,j} &:= \langle \Psi_j^m, \Phi_{c,k}^m \rangle_{\Gamma_c^m}^{(h)}, & [C_c]_{k,\ell} &:= \langle \Phi_{c,\ell}^m, \Phi_{c,k}^m \rangle_{\Gamma_c^m}^{(h)}, \\ [\vec{D}_c]_{k,\ell} &:= \langle \Phi_{c,\ell}^m, \Phi_{c,k}^m \rangle_{\Gamma_c^m}^h \vec{\omega}_{c,\ell}^m, & [\underline{E}_c]_{k,\ell} &:= \langle \nabla_\Gamma \Phi_{c,\ell}^m, \nabla_\Gamma \Phi_{c,k}^m \rangle_{\Gamma_c^m} \end{aligned}$$

for each $c \in \mathbb{N}_{\leq I_S}$.

Generalizing (5.1) to general surface clusters in \mathbb{R}^d , $d = 2, 3$, is now straightforward. The only required changes are to adapt the definition of \underline{P} to the cluster at hand, recall [14], and to let the block matrices be given by $(\vec{N}_{\Omega,\Gamma})_{i,1} := [\beta]_{b_i^-}^{b_i^+} \vec{N}_i$ ($i \in \mathbb{N}_{\leq I_S}$), $(B_{\Omega,\Gamma})_{i,1} := [\beta]_{b_i^-}^{b_i^+} B_i$ ($i \in \mathbb{N}_{\leq I_S}$), $C_\Gamma := \text{diag}(C_i)_{i=1,\dots,I_S}$, $\vec{D}_\Gamma := \text{diag}(\vec{D}_i)_{i=1,\dots,I_S}$ and $\underline{E}_\Gamma := \text{diag}(\varsigma_i \underline{E}_i)_{i=1,\dots,I_S}$.

The linear system (5.1) can either be solved with a Krylov subspace type iterative solver, together with a suitable preconditioner, or it can be reduced with the help of a Schur complement approach. In fact, on following the approach from [13], we can eliminate first κ_ζ^{m+1} and then W^{m+1} , to obtain a linear system just in terms of $\delta \vec{X}^{m+1}$, which can then be solved with preconditioned iterative solvers as in [14]. Similarly to [13], when eliminating W^{m+1} some attention must be placed on the fact that A_Ω has a one-dimensional kernel. We refer to [13] for the precise details.

6 Structure-preserving numerical scheme

In this section, we refine the previously proposed fully discrete scheme (4.4) such that the discrete total energy content is preserved at each time step. To this end, we follow the idea by Bao, Garcke, Nürnberg and Zhao [3] which can interpolate between discrete surface clusters at intermediate timestamps. We define $\Gamma_i^h(t) = \bigcup_{j=1}^{J_i} \overline{\sigma_{i,j}^h(t)}$ as the interpolating polyhedral surfaces where $\{\sigma_{i,j}^h(t)\}_{j=1}^{J_i}$ are mutually disjoint $(d-1)$ -simplices with vertices $\{\vec{q}_{i,k}^h(t)\}_{k=1}^{K_i}$ given by

$$\vec{q}_{i,k}^h(t) = \frac{t_{m+1} - t}{\tau_m} \vec{q}_{i,k}^m + \frac{t - t_m}{\tau_m} \vec{q}_{i,k}^{m+1}, \quad t \in [t_m, t_{m+1}], \quad k = 1, \dots, K_i. \quad (6.1)$$

We now define a discrete normal vector $\vec{\nu}^{m+\frac{1}{2}}$ by

$$\vec{\nu}_i^{m+\frac{1}{2}}|_{\sigma_{i,j}^m} := \frac{1}{\tau_m |\vec{A}\{\sigma_{i,j}^m\}|} \int_{t_m}^{t_{m+1}} \vec{A}\{\sigma_{i,j}^h(t)\} dt \quad \text{for } j \in \mathbb{N}_{\leq J_i} \quad \text{and } i \in \mathbb{N}_{\leq I_S},$$

and the associated vertex normal vector $\vec{\omega}^{m+\frac{1}{2}}$ through

$$\left\langle \vec{\omega}_i^{m+\frac{1}{2}}, \vec{\xi} \right\rangle_{\Gamma_i^m}^h = \left\langle \vec{\nu}_i^{m+\frac{1}{2}}, \vec{\xi} \right\rangle_{\Gamma_i^m} \quad \forall \vec{\xi} \in V^h(\Gamma_i^m), \quad i \in \mathbb{N}_{\leq I_S}.$$

Using the vertex normal vector $\vec{\omega}^{m+\frac{1}{2}}$, we introduce another finite element approximation of (3.3). For each $m \geq 0$, given Γ^m , we find $(W^{m+1}, \vec{X}^{m+1}, \kappa_\zeta^{m+1}) \in S^m \times \underline{V}^h(\Gamma^m) \times V^h(\Gamma^m)$ such that

Motion law: For all $\varphi \in S^m$, it holds that

$$\langle \nabla W^{m+1}, \nabla \varphi \rangle_\Omega + \sum_{i=1}^{I_S} [\beta]_{b_i^-}^{b_i^+} \left\langle \pi_i^h \left[\frac{\vec{X}_i^{m+1} - \text{id}}{\tau_m} \cdot \vec{\omega}_i^{m+\frac{1}{2}} \right], \varphi \right\rangle_{\Gamma_i^m}^{(h)} = 0. \quad (6.2a)$$

Gibbs–Thomson law: For all $\xi \in V^h(\Gamma^m)$, it holds that

$$\langle \kappa_\zeta^{m+1}, \xi \rangle_{\Gamma^m}^h + \sum_{i=1}^{I_S} [\beta]_{b_i^-}^{b_i^+} \langle W^{m+1}, \xi \rangle_{\Gamma_i^m}^{(h)} = 0. \quad (6.2b)$$

Curvature vector: For all $\vec{\eta} \in \underline{V}^h(\Gamma^m)$, it holds that

$$\left\langle \kappa_\zeta^{m+1} \vec{\omega}^{m+\frac{1}{2}}, \vec{\eta} \right\rangle_{\Gamma^m}^h + \left\langle \varsigma \nabla_\Gamma \vec{X}^{m+1}, \nabla_\Gamma \vec{\eta} \right\rangle_{\Gamma^m} = 0. \quad (6.2c)$$

We observe that the only change from (4.4) to (6.2) is that $\vec{\omega}^m$ is now replaced by $\vec{\omega}^{m+\frac{1}{2}}$. Since the latter depends on $\Gamma^{m+1} = \vec{X}^{m+1}(\Gamma^m)$, the scheme (6.2) leads to a nonlinear system of equations, in contrast to (4.4). We shall show that (6.2) preserves the total energy content at each time step. Before proving this, we recall the following lemma from [3, Lemma 3.1] without its proof (see also [40, Lemma 4.4]).

Lemma 6.1. *Let $\vec{X}^{m+1} \in \underline{V}^h(\Gamma^m)$. Then, for every $\ell \in \mathbb{N}_{\leq I_R}$, it holds that*

$$\text{vol}(\mathcal{R}_\ell[\Gamma^{m+1}]) - \text{vol}(\mathcal{R}_\ell[\Gamma^m]) = - \sum_{i=1}^{I_S} \left\langle \left(\vec{X}^{m+1} - \text{id} \right) \cdot \vec{\nu}^{m+\frac{1}{2}}, \chi_{\ell,i} \right\rangle_{\Gamma_i^m},$$

where

$$\chi_{\ell,i} := \begin{cases} 1 & \text{if } b_i^+ = \ell, \\ -1 & \text{if } b_i^- = \ell, \\ 0 & \text{otherwise.} \end{cases}$$

With the help of Lemma 6.1, we can establish the following theorem, where in preparation we define the discrete total energy content as

$$v^m := \sum_{\ell=1}^{I_R} \beta_\ell \text{vol}(\mathcal{R}_\ell[\Gamma^m]) \quad \text{for } m = 0, \dots, M. \quad (6.3)$$

Theorem 6.1. *Let $(W^{m+1}, \vec{X}^{m+1}, \kappa_\varsigma^{m+1}) \in S^m \times \underline{V}^h(\Gamma^m) \times V^h(\Gamma^m)$ be a solution to (6.2). Then it holds that $v^{m+1} = v^m$.*

Proof. We deduce from Lemma 6.1 that

$$\begin{aligned} v^{m+1} - v^m &= \sum_{\ell=1}^{I_R} \beta_\ell \left\{ - \sum_{\substack{i \in \mathbb{N}_{\leq I_S} \\ b_i^+ = \ell}} \left\langle \vec{X}^{m+1} - \text{id}, \vec{\nu}_i^{m+\frac{1}{2}} \right\rangle_{\Gamma_i^m} + \sum_{\substack{i \in \mathbb{N}_{\leq I_S} \\ b_i^- = \ell}} \left\langle \vec{X}^{m+1} - \text{id}, \vec{\nu}_i^{m+\frac{1}{2}} \right\rangle_{\Gamma_i^m} \right\} \\ &= \sum_{\ell=1}^{I_R} \beta_\ell \left\{ - \sum_{\substack{i \in \mathbb{N}_{\leq I_S} \\ b_i^+ = \ell}} \left\langle \vec{X}^{m+1} - \text{id}, \vec{\omega}_i^{m+\frac{1}{2}} \right\rangle_{\Gamma_i^m}^h + \sum_{\substack{i \in \mathbb{N}_{\leq I_S} \\ b_i^- = \ell}} \left\langle \vec{X}^{m+1} - \text{id}, \vec{\omega}_i^{m+\frac{1}{2}} \right\rangle_{\Gamma_i^m}^h \right\} \\ &= -\tau_m \sum_{i=1}^{I_S} [\beta]_{b_i^-}^{b_i^+} \left\langle \pi^h \left[\frac{\vec{X}^{m+1} - \text{id}}{\tau_m} \cdot \vec{\omega}^{m+\frac{1}{2}} \right], 1 \right\rangle_{\Gamma_i^m}^{(h)} = 0. \end{aligned}$$

Here, we have invoked (6.2a) with $\varphi = 1$ to derive the last equality. \square

Remark 6.1. *We observe that as $\vec{\omega}^{m+\frac{1}{2}}$ depends on \vec{X}^{m+1} , the scheme (6.2) is no longer linear. In practice the nonlinear systems of equations arising at each time level of (6.2) can be solved with the aid of a simple lagged iteration as mentioned in [51, §3].*

7 Numerical experiments

In this section, we present numerical experiments to verify the feasibility of the proposed scheme together with its accuracy and efficiency. We implemented the fully discrete finite element approximations (4.4) and (6.2) within the finite element toolbox ALBERTA, see [53]. The arising linear systems of the form (5.1) are either solved with a GMRes iterative solver, applying as preconditioner a least squares solution of the block matrix in (5.1) without the projection matrices \underline{P} . For the computation of the least squares solution we employ the sparse factorization package SPQR, see [27]. Alternatively, and especially in 3d, we solve (5.1) with the help of the previously discussed Schur complement approach. Here we use either UMFPACK, see [26], or a multigrid algorithm for the solution of the arising linear subproblems. We refer to [13] for more details in the two-phase case.

For the triangulation \mathcal{T}^m of the bulk domain Ω , that is used for the bulk finite element space S^m , we use an adaptive mesh with fine elements close to the interface Γ^m and coarser elements away from it. The precise strategy is as described in [13, §5.1] and for a domain $\Omega = (-H, H)^d$, for some $H > 0$, and two integer parameters $N_c < N_f$ results in elements with maximal diameter approximately equal to $h_f = \frac{2H}{N_f}$ close to Γ^m , and elements with maximal diameter approximately equal to $h_c = \frac{2H}{N_c}$ far away from it. Throughout this section, we always set $H = 4$. See Figure 3 for an example adaptive bulk mesh in two space dimensions.

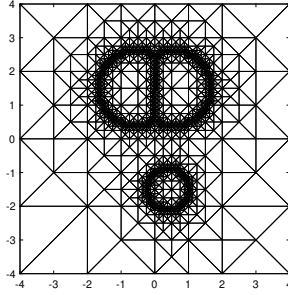


Figure 3: Adaptive bulk mesh in two space dimensions.

We stress that due to the unfitted nature of our finite element approximations, special quadrature rules need to be employed in order to assemble terms that feature both bulk and surface finite element functions. For all the computations presented in this section, we use true integration for these terms, and we refer to [13, 51] for details on the practical implementation. Throughout this section we use (almost) uniform time steps, in that $\tau_m = \tau$ for $m = 0, \dots, M-2$ and $\tau_{M-1} = T - t_{m-1} \leq \tau$. In the sequel, we set all the physical parameters to unity, and in particular $\varsigma_i = 1$ for all $i \in \mathbb{N}_{\leq I_S}$, unless otherwise stated.

7.1 Convergence experiment in 2d

We check the accuracy of the proposed scheme using a rigorous solution to the degenerate multi-phase Stefan problem (1.1) and compare it with the numerical solution. To this end, we consider a curve network which consists of two concentric circles in \mathbb{R}^2 . See Figure 4 for the setting.

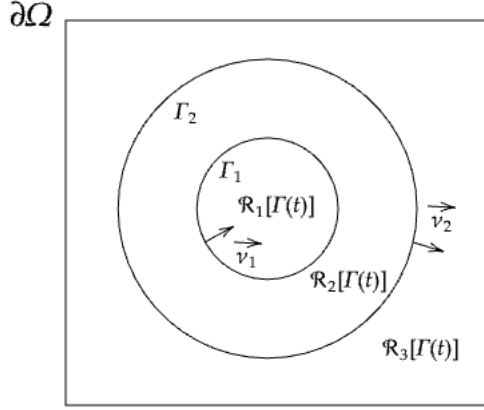


Figure 4: Two concentric circles.

Then, we can obtain the formula of the rigorous solution to the above system as follows:

$$w(x, t) = \begin{cases} -\frac{1}{[\beta]_2^1 R_1(t)} & \text{if } |x| < R_1(t), \\ -\frac{1}{[\beta]_2^1 R_1(t)} + \alpha_2(R_1(t), R_2(t)) \log \frac{|x|}{R_1(t)}, & \text{if } R_1(t) \leq |x| < R_2(t), \\ \frac{1}{[\beta]_2^3 R_2(t)} & \text{if } R_2(t) \leq |x|, \end{cases} \quad (7.1a)$$

where

$$\alpha_2(R_1, R_2) := \frac{\frac{1}{[\beta]_2^1 R_1} + \frac{1}{[\beta]_2^3 R_2}}{\log \frac{R_2}{R_1}} \quad \text{for } R_1, R_2 > 0.$$

We deduce from the motion law that the radii $R_1(t)$ and $R_2(t)$ satisfy the following ordinary differential equations:

$$\begin{aligned} \dot{R}_1(t) &= -\frac{\alpha_2(R_1(t), R_2(t))}{[\beta]_2^1 R_1(t)}, \\ \dot{R}_2(t) &= -\frac{\alpha_2(R_1(t), R_2(t))}{[\beta]_2^3 R_2(t)}, \end{aligned} \quad (7.1b)$$

where \dot{R}_i denotes the time derivative of R_i . In order to make an accurate comparison between true and discrete solution, we prefer to deal with a scalar ordinary differential equation for a single radius. Thanks to Proposition 2.2, we see that the function

$$t \mapsto \pi [\beta]_2^1 R_1(t)^2 - \pi [\beta]_2^3 R_2(t)^2 + \beta_3 \mathcal{L}^2(\Omega),$$

is constant. This implies that $t \mapsto [\beta]_2^1 R_1(t)^2 - [\beta]_2^3 R_2(t)^2$ is also constant. Thus, letting $D_2 := [\beta]_2^1 R_1(0)^2 - [\beta]_2^3 R_2(0)^2$, we obtain

$$\dot{R}_2(t) = -F(R_2(t)) \quad \text{with} \quad F(u) := \frac{\alpha_2\left(\sqrt{\frac{D_2 + [\beta]_2^3 u^2}{[\beta]_2^1}}, u\right)}{[\beta]_2^3 u}, \quad (7.2)$$

where $F(u)$ is defined for every u such that $(D_2 + [\beta]_2^3 u^2)/[\beta]_2^1 > 0$. We can solve (7.2) in terms of the root-finding method as in [33, Eq.(8.2)], namely by finding R_2 such that

$$0 = t + \int_{R_2(0)}^{R_2} \frac{1}{F(u)} du.$$

We show in Figure 5 the evolutions of the radii $R_1(t)$ and $R_2(t)$ satisfying (7.1b), and compare them to the evolutions of the radii of the discrete solution for our scheme (4.4). We note the perfect agreement between the two. For this choice of β , the inner phase shrinks and eventually disappears, leaving a trivial stationary solution for the two-phase problem.

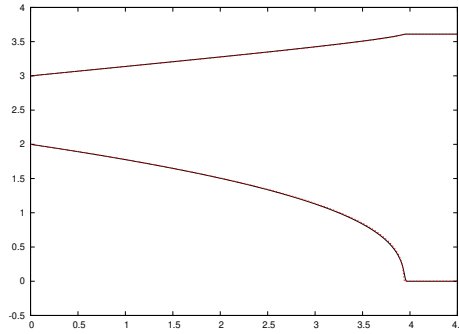


Figure 5: Comparison of the discrete (black, solid) and exact (red, dashed) radii for $(\beta_1, \beta_2, \beta_3) = (-1, 0, 1)$.

The evolution for a different choice of β is shown Figure 6, and we observe that the second phase vanishes as inner and outer circles approach each other to finally only leave a single circular interface that separates phases 1 and 3.

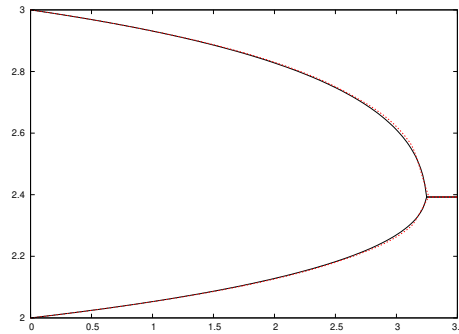


Figure 6: Comparison of the discrete (black, solid) and exact (red, dashed) radii for $(\beta_1, \beta_2, \beta_3) = (-1.6, 0.3, 1.3)$.

In summary, we see from Figure 5 and Figure 6, that setting β_1 to be very small leads to a growth of the inner circle and a shrinking of the outer circle. In fact, it can be seen from (7.1b) that changing the value of β_1 may cause the radius $R_1(t)$ to evolve differently due to the change of the sign of $\dot{R}_1(t)$. It is also easy to check that $\dot{R}_2(t)$ has a different sign to $\dot{R}_1(t)$, and so the outer circle will move in the opposite direction to the inner one.

We perform a convergence experiment for the true solution of (7.1) on the time interval $[0, 1]$. For the discretization parameters, for $i = 0 \rightarrow 4$, we set $N_f = \frac{1}{2}K_\Gamma^0 = 2^{7+i}$, $N_c = 4^i$ and $\tau = 4^{3-i} \times 10^{-3}$. For the discrete solutions of (4.4) and (6.2) we define the errors

$$\|\Gamma^h - \Gamma\|_{L^\infty} = \max_{m=1,\dots,M} \max_{i=1,\dots,I_S} \max_{k=1,\dots,K_i^m} \text{dist}(\vec{q}_{i,k}^m, \Gamma_i(t_m))$$

and

$$\|W^h - w\|_{L^\infty} = \max_{m=1,\dots,M} \|W^m - I^m w(\cdot, t_m)\|_{L^\infty},$$

where $I^m : C(\overline{\Omega}) \rightarrow S^m$ denotes the standard interpolation operator. We also let

$$h_\Gamma^m = \max_{i=1,\dots,I_S} \max_{j=1,\dots,J_i} |\sigma_{i,j}^m|$$

and

$$v_\Delta^M = v^M - v^0,$$

recall (6.3).

We show the errors for the nonlinear scheme (6.2) and for the linear scheme (4.4) in Tables 1 and 2, respectively. Here, we recall that K_Ω^m denotes the degree of freedom of S^m , while K_Γ^m counts the total number of vertices on Γ^m .

h_f	h_Γ^M	$\ W^h - w\ _{L^\infty}$	$\ \Gamma^h - \Gamma\ _{L^\infty}$	K_Ω^M	K_Γ^M	$ v_\Delta^M $
6.2500e-02	1.5401e-01	4.2628e-03	2.0103e-03	2721	256	$< 10^{-10}$
3.1250e-02	7.7011e-02	1.4983e-03	1.9699e-03	5417	512	$< 10^{-10}$
1.5625e-02	3.8502e-02	1.4098e-03	1.3554e-03	10837	1024	$< 10^{-10}$
7.8125e-03	1.9249e-02	7.8872e-04	7.5991e-04	22745	2048	$< 10^{-10}$
3.9062e-03	9.6240e-03	7.7764e-04	4.7532e-04	50417	4096	$< 10^{-10}$

Table 1: Convergence test for (7.1) over the time interval $[0, 1]$ for the scheme (6.2).

h_f	h_Γ^M	$\ W^h - w\ _{L^\infty}$	$\ \Gamma^h - \Gamma\ _{L^\infty}$	K_Ω^M	K_Γ^M	$ v_\Delta^M $
6.2500e-02	1.5394e-01	7.5877e-03	1.8445e-03	2761	256	1.33e-02
3.1250e-02	7.7002e-02	1.5180e-03	1.0028e-03	5433	512	3.44e-03
1.5625e-02	3.8501e-02	1.3572e-03	1.1123e-03	10853	1024	8.64e-04
7.8125e-03	1.9249e-02	7.7496e-04	6.9937e-04	22769	2048	2.15e-04
3.9062e-03	9.6240e-03	7.7408e-04	4.6021e-04	50353	4096	5.37e-05

Table 2: Convergence test for (7.1) over the time interval $[0, 1]$ for the scheme (4.4).

We proceed with another curve network consisting of three concentric circles in \mathbb{R}^2 . Let $R_1(t)$, $R_2(t)$ and $R_3(t)$ be the radii of the three circles at time t with $R_1(t) < R_2(t) < R_3(t)$. See Figure 7 for the setting.

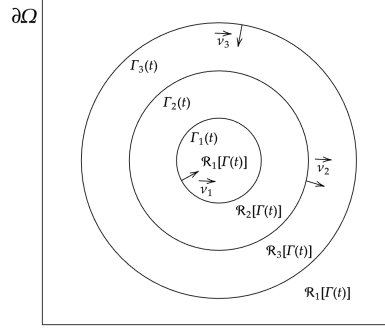


Figure 7: Three concentric circles.

We note that the region $\mathcal{R}_1[\Gamma(t)]$ is not connected in contrast to the previous case (see Figure 4). In this case, we see that $(b_1^+, b_1^-) = (1, 2)$, $(b_2^+, b_2^-) = (3, 2)$ and $(b_3^+, b_3^-) = (3, 1)$, and we have a rigorous solution to (1.1) with $\Gamma(t) = \bigcup_{i=1}^3 \partial B(0, R_i(t))$ as follows:

$$w(x, t) := \begin{cases} -\frac{1}{[\beta]_2^1 R_1(t)} & \text{if } |x| < R_1(t), \\ \frac{\frac{1}{[\beta]_2^3 R_2(t)} + \frac{1}{[\beta]_2^1 R_1(t)}}{\log \frac{R_2(t)}{R_1(t)}} \log \frac{|x|}{R_1(t)} - \frac{1}{[\beta]_2^1 R_1(t)} & \text{if } R_1(t) \leq |x| < R_2(t), \\ \frac{\frac{1}{[\beta]_2^3 R_2(t)} + \frac{1}{[\beta]_1^3 R_3(t)}}{\log \frac{R_2(t)}{R_3(t)}} \log \frac{|x|}{R_3(t)} - \frac{1}{[\beta]_1^3 R_3(t)} & \text{if } R_2(t) \leq |x| < R_3(t), \\ -\frac{1}{[\beta]_1^3 R_3(t)} & \text{if } R_3(t) \leq |x|, \end{cases}$$

with $R_1(t)$, $R_2(t)$ and $R_3(t)$ satisfying the following ordinary differential equations:

$$\begin{aligned} \dot{R}_1(t) &= -\frac{\frac{1}{[\beta]_2^3 R_2(t)} + \frac{1}{[\beta]_2^1 R_1(t)}}{[\beta]_2^1 R_1(t) \log \frac{R_2(t)}{R_1(t)}}, \\ \dot{R}_2(t) &= \frac{1}{[\beta]_2^3 R_2(t)} \left(\frac{\frac{1}{[\beta]_2^3 R_2(t)} + \frac{1}{[\beta]_1^3 R_3(t)}}{\log \frac{R_2(t)}{R_3(t)}} - \frac{\frac{1}{[\beta]_2^3 R_2(t)} + \frac{1}{[\beta]_2^1 R_1(t)}}{\log \frac{R_2(t)}{R_1(t)}} \right), \\ \dot{R}_3(t) &= \frac{\frac{1}{[\beta]_2^3 R_2(t)} + \frac{1}{[\beta]_1^3 R_3(t)}}{[\beta]_1^3 R_3(t) \log \frac{R_2(t)}{R_3(t)}}. \end{aligned} \tag{7.3}$$

We show in Figure 8 a comparison between the solution to (7.3), and the discrete finite element solution to (4.4) that approximates the system (1.1). Once again, we note the excellent agreement between the two. During the evolution, the two innermost disks disappear, leaving a trivial two-phase stationary solution, involving only phases 1 and 3. Observe that once the inner disk vanishes, the remaining radii $R_2(t)$ and $R_3(t)$ satisfy a system of ODEs analogous to (7.1b), involving three phases and two concentric circles.

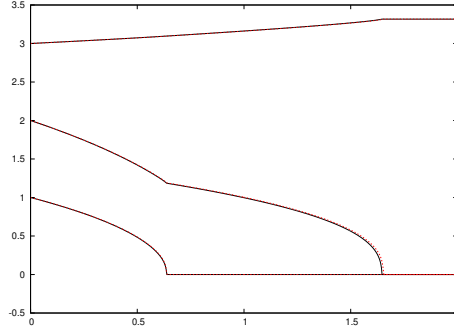


Figure 8: Comparison of the discrete (black, solid) and exact (red, dashed) radii for $(\beta_1, \beta_2, \beta_3) = (-1, 1, 0)$.

7.2 Numerical simulations in 2d

We shall carry out several numerical simulations for the degenerate multi-phase Stefan problem (1.1) in the case $d = 2$.

We begin with a simulation for $(\beta_1, \beta_2, \beta_3) = (0, -1, 1)$ for a stationary solution, that is two separate disks with radii 1 and 0.5, respectively. When the smaller initial radius is smaller than 0.5, the smaller phase disappears. When it is slightly larger than 0.5 it grows and the initially larger phase eventually disappears. We visualize the three different behaviors in Figure 9, where we choose the initially smaller disk to have radius 0.49, 0.5 or 0.51, respectively.

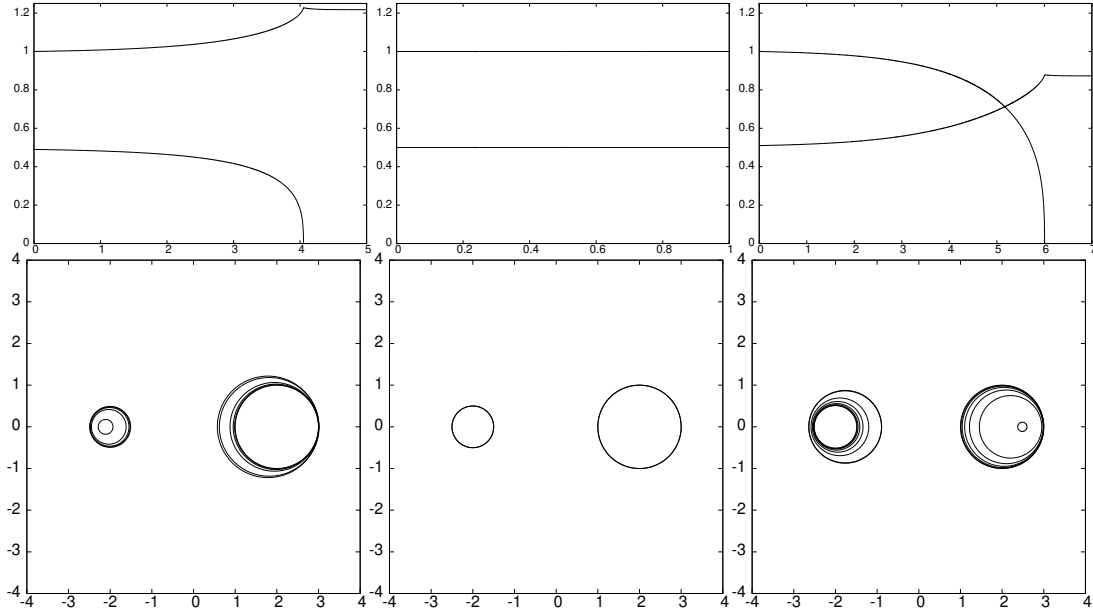


Figure 9: The evolution of half of the maximum extension in x -direction of the two phases over time. For the initial radius 0.49, 0.5 or 0.51 (from left to right) of the initially smaller disk. Below we show plots of the evolutions at times $t = 0, 1, \dots, T$ with $T = 5, 1$ and 7 , respectively.

We proceed with a simple example of a symmetric double bubble in 2d. In this experiment, we set $I_R = 3$, $I_S = 3$, $I_T = 2$, $(\beta_1, \beta_2, \beta_3) = (-1, 0, 1)$, $(b_1^+, b_1^-) = (3, 1)$, $(b_2^+, b_2^-) = (2, 3)$, and $(b_3^+, b_3^-) = (1, 2)$. We show its result in Figure 10 and observe that the left bubble shrinks and the right bubble grows. Eventually, the left bubble vanishes, and the right bubble and the outer phase survive. We note that without heuristic changes of topology our numerical methods would not be able to integrate beyond the vanishing of a (part of) a phase. Hence, we need to perform some simply topological surgery to allow our scheme to continue with the approximation the evolution. To this end, and similarly to our previous work [33], we discard (parts of) phases that have become too small. If such a vanishing part is enclosed by a single curve, it is simply discarded. Otherwise, one of the bounding curves is removed, and the triple junctions it was part of are changed to intersections of the two remaining curves.

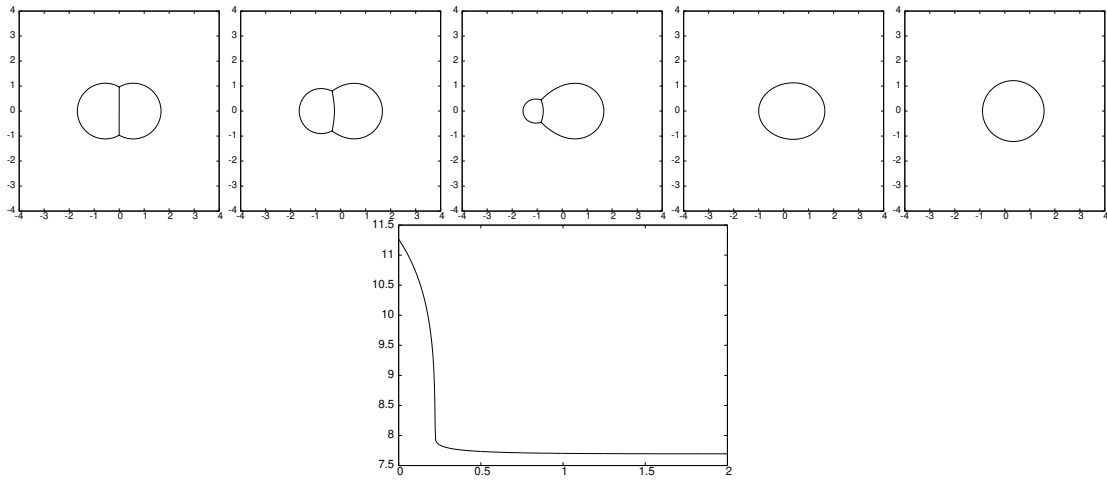


Figure 10: $((\beta_1, \beta_2, \beta_3) = (-1, 0, 1) = \text{right bubble, left bubble, outer phase})$

The solution at times $t = 0, 0.1, 0.2, 0.5, 2$, and a plot of the discrete energy over time.

For this computation, we have $v^0 = 54.6$.

We next carry out a simulation for the same double bubble, but with a different choice of surface tensions. Then, we observe a different behavior of the evolution of the double bubble. In spite of the same choice of β , now the left bubble grows, and the right bubble shrinks and eventually vanishes. We note also that the three contact angles at the triple junctions in this experiment are different from each other, as is to expected from Young's law, see the fourth condition in (1.1), in contrast to the previous case.

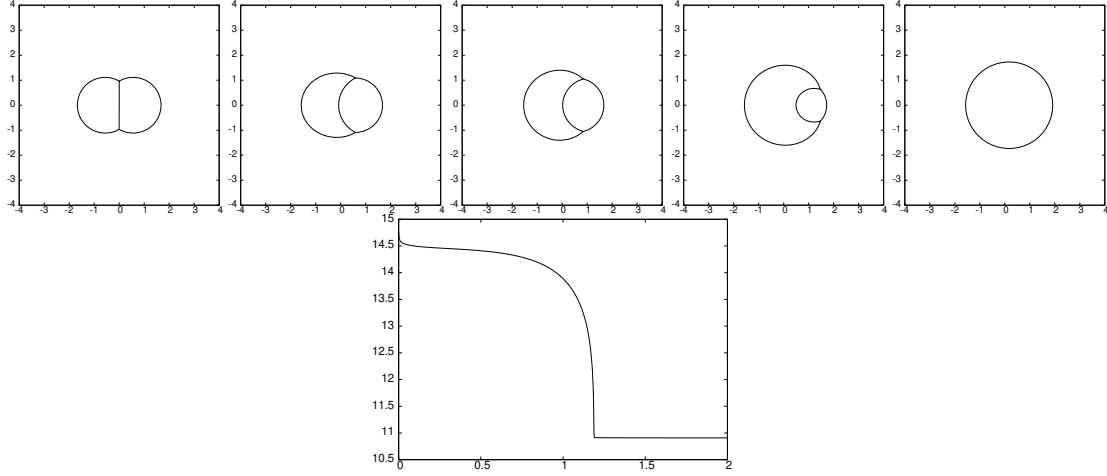


Figure 11: $((\beta_1, \beta_2, \beta_3) = (-1, 0, 1) = \text{right bubble, left bubble, outer phase, and with } \varsigma = (1.75, 1, 1))$. The solution at times $t = 0, 0.2, 0.5, 1, 2$, and a plot of the discrete energy over time. For this computation, we have $v^0 = 54.6$.

In the next set of experiments, we investigate simulations for a standard double bubble, with one of the bubbles making a phase with a separate disk. In particular, we set $I_R = 3$, $I_S = 4$, $I_T = 2$, $(\beta_1, \beta_2, \beta_3) = (0.25, 0, -0.25)$, $(b_1^+, b_1^-) = (3, 1)$, $(b_2^+, b_2^-) = (2, 3)$, $(b_3^+, b_3^-) = (1, 2)$, and $(b_4^+, b_4^-) = (1, 3)$. The two bubbles of the double bubble enclose an area about 3.139 each, while the disk has an initial radius of $\frac{8}{5}$, meaning it initially encloses an area of $\frac{25\pi}{64} \approx 1.227$. During the evolution, the left bobble shrinks, while the right bubble grows correspondingly. Eventually, the left bobble vanishes, and the right bubble and the disk survive. These survivors enclose the same phase, and the disk is absorbed by the right bubble according to the energy minimization. See Figure 12 for the results.

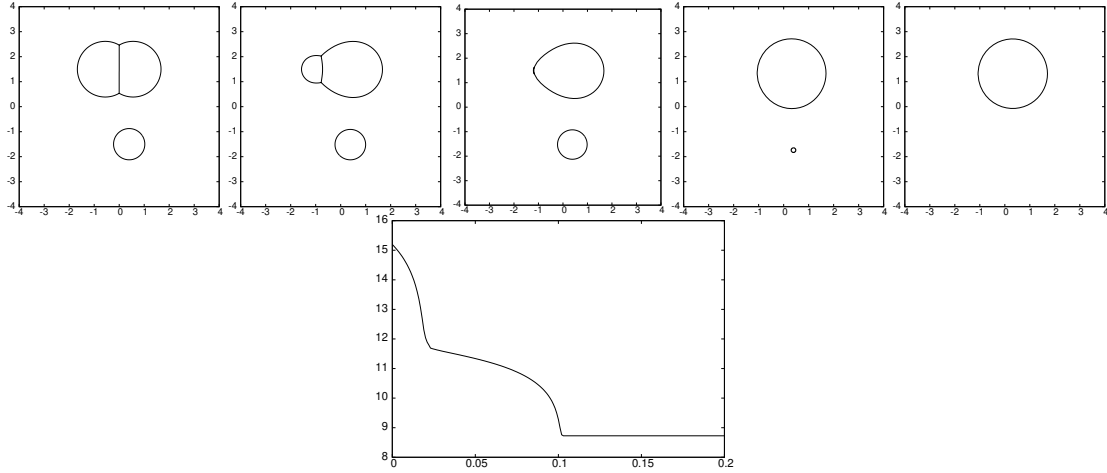


Figure 12: $((\beta_1, \beta_2, \beta_3) = (0.25, 0, -0.25) = \text{right bubble plus disk, left bubble, outer phase})$. The solution at times $t = 0, 0.015, 0.02, 0.1, 0.2$, and a plot of the discrete energy over time. For this computation, we have $v^0 = -13$.

We repeat the same experiment with the disk which encloses a larger area, namely its

radius is set as $\frac{5}{4}$ so that it encloses an area of $\frac{25\pi}{16} \approx 4.909$. Then, as in the previous case, the left bubble shrinks and vanishes, and the right bubble and the disk survive. However, to obey the energy minimization, the disk eventually absorbs the right bubble. See Figure 13 for the results.

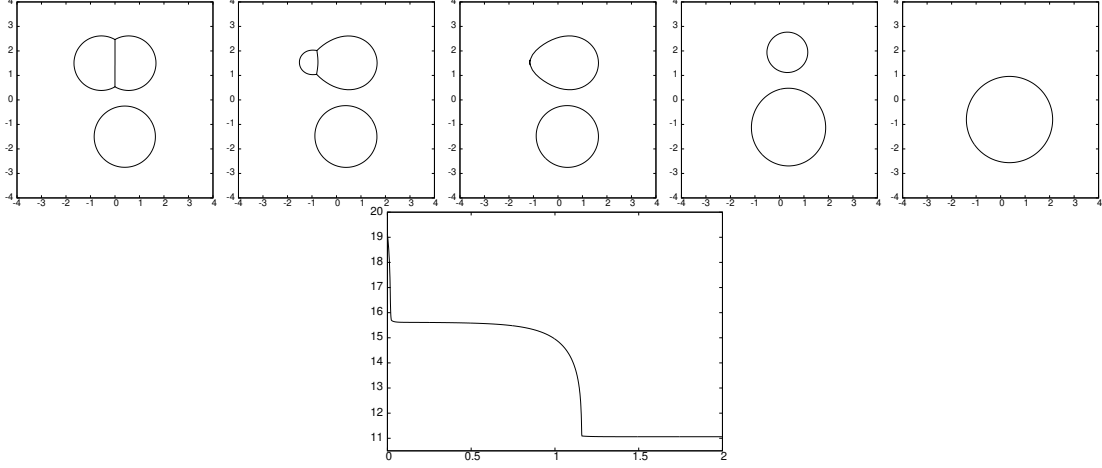


Figure 13: $((\beta_1, \beta_2, \beta_3) = (0.25, 0, -0.25) = \text{right bubble plus disk, left bubble, outer phase})$
The solution at times $t = 0, 0.015, 0.02, 1, 2$, and a plot of the discrete energy over time.
For this computation, we have $v^0 = -11.2$.

7.3 Convergence experiment in 3d

We consider the 3d equivalent of the setup displayed in Figure 4. For the case $d = 3$, we have the rigorous solution to the three-phase system as follows:

$$w(x, t) = \begin{cases} -\frac{2}{[\beta]_2^1 R_1(t)} & \text{if } |x| < R_1(t), \\ -\frac{2}{[\beta]_2^1 R_1(t)} - \frac{2\alpha_3(R_1(t), R_2(t))}{R_1(t)} + \frac{2\alpha_3(R_1(t), R_2(t))}{|x|} & \text{if } R_1(t) \leq |x| < R_2(t), \\ \frac{2}{[\beta]_2^3 R_2(t)} & \text{if } R_2(t) \leq |x|, \end{cases}$$

where

$$\alpha_3(R_1, R_2) := \frac{\frac{1}{[\beta]_2^1 R_1} + \frac{1}{[\beta]_2^3 R_2}}{\frac{1}{R_2} - \frac{1}{R_1}} \quad \text{for } R_1, R_2 > 0.$$

The formulae for $R_1(t)$ and $R_2(t)$ are given as the solutions to the following system of ordinary differential equations:

$$\begin{aligned} \dot{R}_1(t) &= \frac{2\alpha_3(R_1(t), R_2(t))}{[\beta]_2^1 R_1(t)^2}, \\ \dot{R}_2(t) &= \frac{2\alpha_3(R_1(t), R_2(t))}{[\beta]_2^3 R_2(t)^2}. \end{aligned}$$

Proposition 2.2 again implies that the function $t \mapsto [\beta]_2^1 R_1(t)^3 - [\beta]_2^3 R_2(t)^3$ is constant, and hence we can solve the above system as in the case $d = 2$. Namely, we have the ordinary

differential equation for $R_2(t)$ as

$$\dot{R}_2(t) = -F(R_2(t)), \quad F(u) := -\frac{2 \alpha_3 \left(\sqrt[3]{\frac{D_3 + [\beta]_2^3 u^3}{[\beta]_2^1}}, u \right)}{[\beta]_2^3 u^2} \quad (7.4)$$

with $D_3 := [\beta]_2^1 R_1(0)^3 - [\beta]_2^3 R_2(0)^3$. We show in Figure 14 the result of accuracy check for the formulae for $R_1(t)$ and $R_2(t)$.

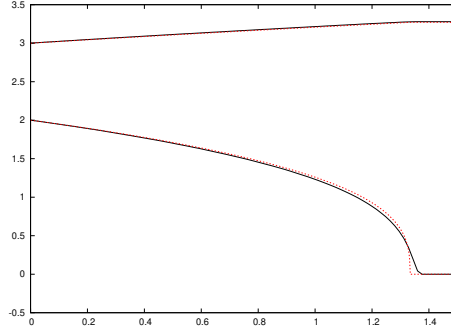


Figure 14: Comparison of the discrete (black, solid) and exact (red, dashed) radii for $(\beta_1, \beta_2, \beta_3) = (-1, 0, 1)$.

We also perform a convergence experiment for the true solution of (7.4) for $d = 3$ over the time interval $[0, 0.5]$. For $i = 0 \rightarrow 3$, we set $N_f = 2^{5+i}$, $N_c = 4^i$ and $\frac{1}{2}K_\Gamma^0 = \hat{K}(i)$, where $(\hat{K}(0), \hat{K}(1), \hat{K}(2), \hat{K}(3)) = (770, 3074, 12290, 49154)$, and $\tau = 4^{3-i} \times 10^{-3}$. The errors $\|W^h - w\|_{L^\infty}$ and $\|\Gamma^h - \Gamma\|_{L^\infty}$ are displayed in Tables 3 and 4.

h_f	h_Γ^M	$\ W^h - w\ _{L^\infty}$	$\ \Gamma^h - \Gamma\ _{L^\infty}$	K_Ω^M	K_Γ^M	$ v_\Delta^M $
2.5000e-01	6.4741e-01	5.1264e-02	4.3538e-02	11043	1540	$< 10^{-10}$
1.2500e-01	3.2398e-01	3.3996e-02	1.9571e-02	45469	6148	$< 10^{-10}$
6.2500e-02	1.6204e-01	1.5014e-02	9.6263e-03	188931	24580	$< 10^{-10}$

Table 3: Convergence test for (7.4) over the time interval $[0, 0.5]$ for the scheme (4.4).

h_f	h_Γ^M	$\ W^h - w\ _{L^\infty}$	$\ \Gamma^h - \Gamma\ _{L^\infty}$	K_Ω^M	K_Γ^M	$ v_\Delta^M $
2.5000e-01	6.4636e-01	2.4897e-02	1.3525e-02	11043	1540	3.17e-01
1.2500e-01	3.2393e-01	2.7050e-02	1.2229e-02	45661	6148	8.18e-02
6.2500e-02	1.6207e-01	1.1793e-02	7.8416e-03	189027	24580	2.02e-02
3.1250e-02	8.1017e-02	7.1962e-03	4.2435e-03	787657	98308	4.95e-03

Table 4: Convergence test for (7.4) over the time interval $[0, 0.5]$ for the scheme (6.2).

7.4 Numerical simulations in 3d

We consider a three-dimensional analogue of the simulation shown in Figure 10, that is for a standard double bubble in 3d. In this experiment, we set $I_R = 3$, $I_S = 3$, $I_T = 1$,

$(\beta_1, \beta_2, \beta_3) = (-0.1, 0, 0.1)$, $(b_1^+, b_1^-) = (3, 1)$, $(b_2^+, b_2^-) = (2, 3)$, and $(b_3^+, b_3^-) = (1, 2)$. See Figure 15 for the evolution, where we observe that the second phases vanishes extremely quickly.

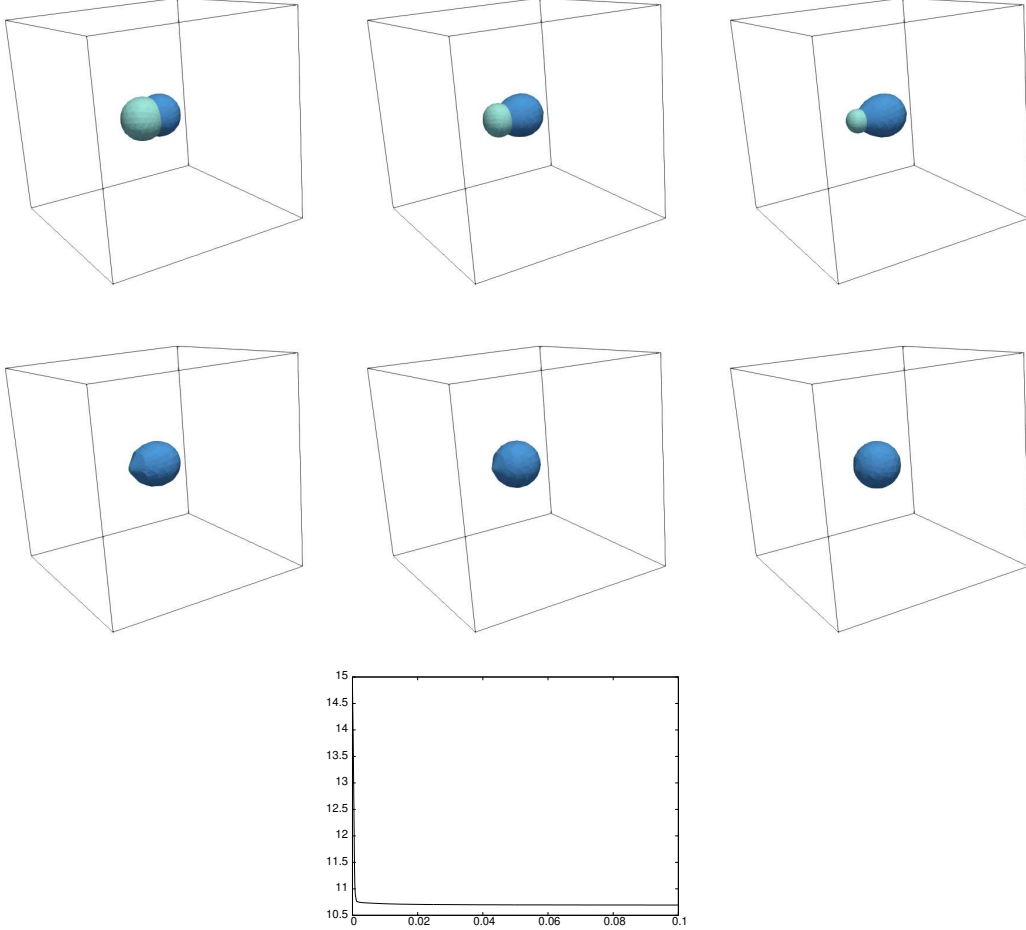


Figure 15: $((\beta_1, \beta_2, \beta_3) = (-0.1, 0, 0.1) = \text{right bubble, left bubble, outer phase})$
The solution at times $t = 0, 0.0002, 0.0003, 0.001, 0.01, 0.1$, and a plot of the discrete energy over time. For this computation, we have $v^0 = 50.6$.

8 Conclusion

In this paper, we have proposed numerical methods for the degenerate multi-phase Stefan problem (1.1) in two and three space dimensions. The approach is based on the parametric finite element method and can deal with several phases and the presence of triple junctions. Overall we have introduced two schemes: a linear one and a nonlinear one. Both schemes can be shown to be unconditionally stable, while the nonlinear one in addition also conserves the total energy content. Moreover, we have carried out numerical experiments which show the practicality and accuracy of the introduced methods.

References

- [1] H. ABELS, M. RAUCHECKER, AND M. WILKE, Well-posedness and qualitative behaviour of the Mullins-Sekerka problem with ninety-degree angle boundary contact, Math. Ann., 381 (2021), pp. 363–403.
- [2] E. BÄNSCH, K. DECKELNICK, H. GARCKE, AND P. POZZI, Interfaces: Modeling, Analysis, Numerics, Oberwolfach Seminars, Birkhäuser Cham, 2023.
- [3] W. BAO, H. GARCKE, R. NÜRNBERG, AND Q. ZHAO, A structure-preserving finite element approximation of surface diffusion for curve networks and surface clusters, Numer. Methods Partial Differ. Eq., 39 (2023), pp. 759–794.
- [4] W. BAO AND Y. LI, A symmetrized parametric finite element method for anisotropic surface diffusion in three dimensions, SIAM J. Sci. Comput., 45 (2023), pp. A1438–A1461.
- [5] —, A structure-preserving parametric finite element method for geometric flows with anisotropic surface energy, Numer. Math., 156 (2024), pp. 609–639.
- [6] W. BAO AND Q. ZHAO, A structure-preserving parametric finite element method for surface diffusion, SIAM J. Numer. Anal., 59 (2021), pp. 2775–2799.
- [7] J. W. BARRETT AND J. F. BLOWEY, An error bound for the finite element approximation of the Cahn-Hilliard equation with logarithmic free energy, Numer. Math., 72 (1995), pp. 1–20.
- [8] J. W. BARRETT, J. F. BLOWEY, AND H. GARCKE, Finite element approximation of the Cahn-Hilliard equation with degenerate mobility, SIAM J. Numer. Anal., 37 (1999), pp. 286–318.
- [9] —, On fully practical finite element approximations of degenerate Cahn-Hilliard systems, M2AN Math. Model. Numer. Anal., 35 (2001), pp. 713–748.
- [10] J. W. BARRETT, H. GARCKE, AND R. NÜRNBERG, On the variational approximation of combined second and fourth order geometric evolution equations, SIAM J. Sci. Comput., 29 (2007), pp. 1006–1041.
- [11] J. W. BARRETT, H. GARCKE, AND R. NÜRNBERG, A parametric finite element method for fourth order geometric evolution equations, J. Comput. Phys., 222 (2007), pp. 441–462.
- [12] J. W. BARRETT, H. GARCKE, AND R. NÜRNBERG, Finite element approximation of coupled surface and grain boundary motion with applications to thermal grooving and sintering, European J. Appl. Math., 21 (2010), pp. 519–556.
- [13] J. W. BARRETT, H. GARCKE, AND R. NÜRNBERG, On stable parametric finite element methods for the Stefan problem and the Mullins-Sekerka problem with applications to dendritic growth, J. Comput. Phys., 229 (2010), pp. 6270–6299.
- [14] J. W. BARRETT, H. GARCKE, AND R. NÜRNBERG, Parametric approximation of surface clusters driven by isotropic and anisotropic surface energies, Interfaces Free Bound., 12 (2010), pp. 187–234.

- [15] J. W. BARRETT, H. GARCKE, AND R. NÜRNBERG, Parametric finite element approximations of curvature-driven interface evolutions, *Handb. Numer. Anal.*, 21 (2020), pp. 275–423.
- [16] P. BATES, X. CHEN, AND X. DENG, A numerical scheme for the two phase Mullins-Sekerka problem, *Electronic Journal of Differential Equations*, 1995 (1995), pp. 1–27.
- [17] P. W. BATES AND S. BROWN, A numerical scheme for the Mullins-Sekerka evolution in three space dimensions, in *Differential equations and computational simulations* (Chengdu, 1999), World Sci. Publ., River Edge, NJ, 2000, pp. 12–26.
- [18] J. F. BLOWEY, M. I. M. COPETTI, AND C. M. ELLIOTT, Numerical analysis of a model for phase separation of a multi-component alloy, *IMA J. Numer. Anal.*, 16 (1996), pp. 111–139.
- [19] J. F. BLOWEY AND C. M. ELLIOTT, The Cahn-Hilliard gradient theory for phase separation with nonsmooth free energy. II. Numerical analysis, *European J. Appl. Math.*, 3 (1992), pp. 147–179.
- [20] E. BRETIN, R. DENIS, S. MASNOU, A. SENGERS, AND G. TERII, A multiphase Cahn-Hilliard system with mobilities and the numerical simulation of dewetting, *ESAIM Math. Model. Numer. Anal.*, 57 (2023), pp. 1473–1509.
- [21] L. BRONSARD, H. GARCKE, AND B. STOTH, A multi-phase Mullins-Sekerka system: matched asymptotic expansions and an implicit time discretisation for the geometric evolution problem, *Proc. Roy. Soc. Edinburgh Sect. A*, 128 (1998), pp. 481–506.
- [22] A. CHAMBOLLE AND T. LAUX, Mullins-Sekerka as the Wasserstein flow of the perimeter, *Proc. Amer. Math. Soc.*, 149 (2021), pp. 2943–2956.
- [23] C. CHEN, C. KUBLIK, AND R. TSAI, An implicit boundary integral method for interfaces evolving by Mullins-Sekerka dynamics, in *Mathematics for nonlinear phenomena—analysis and computation*, vol. 215 of *Springer Proc. Math. Stat.*, Springer, Cham, 2017, pp. 1–21.
- [24] S. CHEN, B. MERRIMAN, S. OSHER, AND P. SMEREKA, A simple level set method for solving Stefan problems, *J. Comput. Phys.*, 135 (1997), pp. 8–29.
- [25] X. CHEN, J. HONG, AND F. YI, Existence, uniqueness, and regularity of classical solutions of the Mullins-Sekerka problem, *Comm. Partial Differential Equations*, 21 (1996), pp. 1705–1727.
- [26] T. A. DAVIS, Algorithm 832: UMFPACK V4.3—an unsymmetric-pattern multifrontal method, *ACM Trans. Math. Software*, 30 (2004), pp. 196–199.
- [27] T. A. DAVIS, Algorithm 915, SuiteSparseQR: Multifrontal multithreaded rank-revealing sparse QR factorization, *ACM Trans. Math. Software*, 38 (2011), pp. 1–22.
- [28] C. M. ELLIOTT AND D. A. FRENCH, Numerical studies of the Cahn-Hilliard equation for phase separation, *IMA J. Appl. Math.*, 38 (1987), pp. 97–128.

- [29] J. ESCHER, A.-V. MATIOC, AND B.-V. MATIOC, The Mullins-Sekerka problem via the method of potentials, Math. Nachr., 297 (2024), pp. 1960–1977.
- [30] J. ESCHER AND G. SIMONETT, Classical solutions for Hele-Shaw models with surface tension, Adv. Differential Equations, 2 (1997), pp. 619–642.
- [31] J. ESCHER AND G. SIMONETT, A center manifold analysis for the Mullins-Sekerka model, J. Differential Equations, 143 (1998), pp. 267–292.
- [32] T. ETO, A rapid numerical method for the Mullins-Sekerka flow with application to contact angle problems, J. Sci. Comput., 98 (2024), p. 63.
- [33] T. ETO, H. GARCKE, AND R. NÜRNBERG, A structure-preserving finite element method for the multi-phase Mullins-Sekerka problem with triple junctions, Numer. Math., 156 (2024), pp. 1479–1509.
- [34] D. J. EYRE, Systems of Cahn-Hilliard equations, SIAM J. Appl. Math., 53 (1993), pp. 1686–1712.
- [35] X. FENG AND A. PROHL, Error analysis of a mixed finite element method for the Cahn-Hilliard equation, Numer. Math., 99 (2004), pp. 47–84.
- [36] X. FENG AND A. PROHL, Numerical analysis of the Cahn-Hilliard equation and approximation of the Hele-Shaw problem, Interfaces Free Bound., 7 (2005), pp. 1–28.
- [37] J. FISCHER, S. HENSEL, T. LAUX, AND T. M. SIMON, A weak-strong uniqueness principle for the Mullins-Sekerka equation, arXiv preprint arXiv:2404.02682, (2024).
- [38] H. GARCKE, Curvature driven interface evolution, Jahresber. Dtsch. Math.-Ver., 115 (2013), pp. 63–100.
- [39] H. GARCKE, R. NÜRNBERG, AND Q. ZHAO, Structure-preserving discretizations of two-phase Navier-Stokes flow using fitted and unfitted approaches, J. Comput. Phys., 489 (2023), p. 112276.
- [40] H. GARCKE, R. NÜRNBERG, AND Q. ZHAO, A variational front-tracking method for multiphase flow with triple junctions, Math. Comp., (2025), pp. 1–36.
- [41] H. GARCKE AND M. RAUCHECKER, Stability analysis for stationary solutions of the Mullins-Sekerka flow with boundary contact, Math. Nachr., 295 (2022), pp. 683–705.
- [42] H. GARCKE AND T. STURZENHECKER, The degenerate multi-phase Stefan problem with Gibbs-Thomson law, Adv. Math. Sci. Appl., 8 (1998), pp. 929–941.
- [43] S. HENSEL AND K. STINSON, Weak solutions of Mullins-Sekerka flow as a Hilbert space gradient flow, Arch. Ration. Mech. Anal., 248 (2024), p. 8.
- [44] F. IZSÁK AND T.-E. DJEBBAR, Learning Data for Neural-Network-Based Numerical Solution of PDEs: Application to Dirichlet-to-Neumann Problems, Algorithms, 16 (2023), p. 111.
- [45] M. LI AND Q. ZHAO, Parametric finite element approximations for anisotropic surface diffusion with axisymmetric geometry, J. Comput. Phys., 497 (2024), p. 112632.

- [46] Y. LI, J. CHOI, AND J. KIM, Multi-component Cahn-Hilliard system with different boundary conditions in complex domains, J. Comput. Phys., 323 (2016), pp. 1–16.
- [47] Y. LI, R. LIU, Q. XIA, C. HE, AND Z. LI, First- and second-order unconditionally stable direct discretization methods for multi-component Cahn-Hilliard system on surfaces, J. Comput. Appl. Math., 401 (2022), p. 113778.
- [48] S. LUCKHAUS AND T. STURZENHECKER, Implicit time discretization for the mean curvature flow equation, Calc. Var. Partial Differential Equations, 3 (1995), pp. 253–271.
- [49] U. F. MAYER, A numerical scheme for moving boundary problems that are gradient flows for the area functional, European J. Appl. Math., 11 (2000), pp. 61–80.
- [50] R. NÜRNBERG, Numerical simulations of immiscible fluid clusters, Appl. Numer. Math., 59 (2009), pp. 1612–1628.
- [51] ———, A structure preserving front tracking finite element method for the Mullins–Sekerka problem, J. Numer. Math., 31 (2023), pp. 137–155.
- [52] M. RÖGER, Existence of weak solutions for the Mullins-Sekerka flow, SIAM J. Math. Anal., 37 (2005), pp. 291–301.
- [53] A. SCHMIDT AND K. G. SIEBERT, Design of Adaptive Finite Element Software: The Finite Element Toolbox ALBERTA, vol. 42 of Lecture Notes in Computational Science and Engineering, Springer-Verlag, Berlin, 2005.
- [54] S. SERFATY, Gamma-convergence of gradient flows on Hilbert and metric spaces and applications, Discrete Contin. Dyn. Syst., 31 (2011), pp. 1427–1451.
- [55] J. ZHU, X. CHEN, AND T. HOU, An Efficient Boundary Integral Method for the Mullins–Sekerka Problem, J. Comput. Phys., 127 (1996), pp. 246–267.